Brain, Behavior, and Immunity 101 (2022) 194–210

Contents lists available at ScienceDirect

Brain Behavior and Immunity

journal homepage: www.elsevier.com/locate/ybrbi

Full-length Article

Neurodegeneration by α-synuclein-specific T cells in AAV-A53T-α-synuclein Parkinson's disease mice

Akua A. Karikari [a], Rhonda L. McFleder [a], Eliana Ribechini [b], Robert Blum [c], Valentin Bruttel [d], Susanne Knorr [a], Mona Gehmeyr [a], Jens Volkmann [a], Jonathan M. Brotchie [e], Fadhil Ahsan [d], Beatrice Haack [d], Camelia-Maria Monoranu [f], Ursula Keber [g], Rima Yeghiazaryan [g], Axel Pagenstecher [g], Tobias Heckel [h], Thorsten Bischler [h], Jörg Wischhusen [d], James B. Koprich [e], Manfred B. Lutz [b,*], Chi Wang Ip [a,*]

[a] Department of Neurology, University Hospital of Würzburg, Würzburg, Germany
[b] Institute for Virology and Immunobiology, University of Würzburg, Würzburg, Germany
[c] Institute of Clinical Neurobiology, University Hospital of Würzburg, Würzburg, Germany
[d] Section for Experimental Tumor Immunology, Department of Obstetrics and Gynecology, University Hospital of Würzburg, Würzburg, Germany
[e] Krembil Research Institute, Toronto Western Hospital, University Health Network, Toronto, ON, Canada
[f] Institute of Pathology, Department of Neuropathology, University of Würzburg, Würzburg, Germany
[g] Department of Neuropathology, Philipps University and University Hospital of Marburg, Marburg, Germany
[h] Core Unit Systems Medicine, University of Würzburg, Würzburg, Germany

ARTICLE INFO

Keywords:
Parkinson's disease
Neuroinflammation
T cells
Antigen-specificity
α-synuclein

ABSTRACT

Background: Antigen-specific neuroinflammation and neurodegeneration are characteristic for neuroimmunological diseases. In Parkinson's disease (PD) pathogenesis, α-synuclein is a known culprit. Evidence for α-synuclein-specific T cell responses was recently obtained in PD. Still, a causative link between these α-synuclein responses and dopaminergic neurodegeneration had been lacking. We thus addressed the functional relevance of α-synuclein-specific immune responses in PD in a mouse model.

Methods: We utilized a mouse model of PD in which an Adeno-associated Vector 1/2 serotype (AAV1/2) expressing human mutated A53T-α-Synuclein was stereotactically injected into the substantia nigra (SN) of either wildtype C57BL/6 or Recombination-activating gene 1 $(RAG1)^{-/-}$ mice. Brain, spleen, and lymph node tissues from different time points following injection were then analyzed via FACS, cytokine bead assay, immunohistochemistry and RNA-sequencing to determine the role of T cells and inflammation in this model. Bone marrow transfer from either $CD4^+/CD8^-$, $CD4^-/CD8^+$, or $CD4^+/CD8^+$ $(JHD^{-/-})$ mice into the RAG-$1^{-/-}$ mice was also employed. In addition to the *in vivo* studies, a newly developed A53T-α-synuclein-expressing neuronal cell culture/immune cell assay was utilized.

Results: AAV-based overexpression of pathogenic human A53T-α-synuclein in dopaminergic neurons of the SN stimulated T cell infiltration. RNA-sequencing of immune cells from PD mouse brains confirmed a pro-inflammatory gene profile. T cell responses were directed against A53T-α-synuclein-peptides in the vicinity of position 53 (68–78) and surrounding the pathogenically relevant S129 (120–134). T cells were required for α-synuclein-induced neurodegeneration *in vivo* and *in vitro,* while B cell deficiency did not protect from dopaminergic neurodegeneration.

Conclusions: Using T cell and/or B cell deficient mice and a newly developed A53T-α-synuclein-expressing neuronal cell culture/immune cell assay, we confirmed *in vivo* and *in vitro* that pathogenic α-synuclein peptide-specific T cell responses can cause dopaminergic neurodegeneration and thereby contribute to PD-like pathology.

Abbreviations: PD, Parkinson's Disease; SN, Substantia Nigra; TNF, Tumor Necrosis Factor; IL, Interleukin; MPTP, 1-methyl-4-phenyl-1,2,3,6-tetrahydropyridine; 6-OHDA, 6-hydroxy dopamine; AAV1/2, Adeno-associated virus serotype 1/2; haSyn, Human pathogenic A53T-α-synuclein; EV, Empty Vector; GO, Gene Ontology; RAG-1, Recombination-activating gene 1 RAG-1; BM, Bone Marrow; DAT, Dopamine Transporter; HVA, Homovanilic Acid; DA, Dopamine; IFN, Interferon; DOPAC, 3,4-dihydroxyphenylacetic acid; CTCF, Corrected Total Cell Fluorescence.

* Corresponding authors.
E-mail addresses: m.lutz@vim.uni-wuerzburg (M.B. Lutz), ip_c@ukw.de (C.W. Ip).

https://doi.org/10.1016/j.bbi.2022.01.007
Received 11 June 2021; Received in revised form 5 January 2022; Accepted 8 January 2022
Available online 12 January 2022

1. Background

Parkinson's disease (PD) is the most common neurodegenerative movement disorder, affecting 6–7 million people worldwide. Pathologic hallmarks are degeneration of dopaminergic neurons in the substantia nigra (SN) and formation of α-synuclein-containing protein aggregates called Lewy-bodies (Spillantini et al., 1997). While the physiological role of α-synuclein points towards a function in synaptic transmitter release (Abeliovich et al., 2000), the pathogenic role of insoluble α-synuclein remains obscure (Bendor et al., 2013). The observation that multiplications and mutations of the α-synuclein encoding SNCA gene can elicit genetically inherited forms of PD has robustly linked α-synuclein to PD pathogenesis (Fuchs et al., 2007; Kruger et al., 1998; Polymeropoulos et al., 1997). Though generally not considered an autoimmune disease, neuroinflammation still plays an essential role in the pathogenesis of PD. The SN of *post mortem* human PD brains is characterized by microglia activation and T cell infiltration (Brochard et al., 2009; McGeer et al., 1988). Additionally, pro-inflammatory cytokines such as tumor necrosis factor (TNF)-α, interferon (IFN)-γ, interleukins (IL)-1β and IL-6 are elevated in the nigrostriatal tract of PD patients compared to controls (Mogi et al., 1994a; Mogi et al., 1994b). Naïve T cells and anti-inflammatory regulatory T cells are decreased in the peripheral blood of PD patients (Bas et al., 2001; Saunders et al., 2012). An increased ratio of IFN-γ to IL-4-producing T cells in PD patients indicates a shift towards a pro-inflammatory environment (Baba et al., 2005). Recently, α-synuclein-specific T cell responses were detected in peripheral blood cells of PD patients (Sulzer et al., 2017) and found to precede motor symptoms (Lindestam Arlehamn et al., 2020). Two α-synuclein-deduced peptides were shown to elicit MHC-restricted cytokine release from peripheral blood mononuclear cells (Sulzer et al., 2017). One antigenic region (Y39) is close to well-known disease-associated α-synuclein mutations, such as the A53T mutation (Hernandez et al., 2016; Sulzer et al., 2017). The second antigenic region surrounds the phosphorylated S129 position. Extensive S129 phosphorylation, which promotes α-synuclein fibril formation, is considered a specific marker of α-synucleinopathies (Fujiwara et al., 2002). However, whether immunogenic variants of α-synuclein and α-synuclein-specific T cells contribute functionally to neurodegeneration and disease progression in PD was unclear.

The pathogenic role of T cells in PD has mostly been analyzed in toxin-based models such as the 1-methyl-4-phenyl-1,2,3,6-tetrahydropyridine (MPTP) or the 6-hydroxy dopamine (6-OHDA) models (Brochard et al., 2009; Ip et al., 2015; Reynolds et al., 2010). However, given their lack of α-synuclein aggregation and Lewy body formation, these models poorly reflect the molecular aspects of the human disease. The role of the adaptive immune system thus needs to be assessed in pathogenetically more relevant model systems. Williams et al. recently tested the role of T cells in a viral vector model of PD. However, the antigen specificities of these cells were not evaluated (Williams et al., 2021). We have recently generated a mouse model of PD, in which neurodegeneration is induced by stereotactic injection of a viral vector (AAV1/2) encoding the human pathogenic A53T-α-synuclein (haSyn) in the SN (Ip et al., 2017). This haSyn PD model displays a high face and construct validity with behavioral deficits, loss of dopaminergic SN neurons and striatal fibers, reduction of striatal dopamine, and formation of insoluble α-synuclein aggregates after proteinase K digestion. These aggregates show $aSyn^{S129}$ phosphorylation and Lewy-like neurites and bodies. Here we confirm that T cells found in brains of haSyn PD mice induce neurodegeneration with PD-like symptoms. We describe novel putatively MHC I- and MHC II-restricted haSyn peptides that induce IFN-γ release from brain, cervical lymph nodes and splenic T cells from diseased mice. Building on the recent descriptions of α-synuclein-specific immune responses in patients with PD (Gate et al., 2021; Lindestam Arlehamn et al., 2020; Sulzer et al., 2017) and on negative correlations between immunosuppression and the risk for PD (Racette et al., 2018), our findings support immunomodulation as a neuroprotective strategy in PD.

2. Material and methods

2.1. Human midbrain sections

Human brains were obtained with the written informed consent of the next of kin and according to the guidelines of the Local Ethics Committee of the University Hospital of Marburg. Formalin-fixed and paraffin-embedded archival human brain tissue from the SN pars compacta from neuropathologically characterized PD cases (n = 22 SN from 11 patients, Braak stage 4: n = 3, stage 5: n = 4, stage 6: n = 4, (Braak et al., 2004), mean age 73.5 years ± 11.9 S.D.) and age-matched controls (n = 18 SN from 9 controls, Braak stage 0, 69.7 ± 12.0 years) were collected from the Department of Neuropathology Marburg. The male/female ratio in the control group was 8/1, in the PD group 7/4. Immunohistochemistry was performed on 3 μm thick sections with rabbit anti-CD4 (1:50; DCS diagnostics CI851C002; clone SP35), rabbit anti-CD8 (1:100; DCS diagnostics CI008C002; clone SP16) and mouse anti-CD68 (1:100; Dako M0876; clone PG-M1). $CD4^+$ and $CD8^+$ cells were counted within the whole SN using 40x magnification. The area of $CD68^+$ microglial processes and macrophages was measured in 10 representative areas of 0.036 mm^2 each equally distributed in the SN using the NIH ImageJ Software.

2.2. Double immunofluorescence for $CD8^+$ T cells and activation markers in human midbrain sections

Double immunofluorescence-stainings were performed on 3 μm thick sections with either rabbit anti-CD8 or mouse anti-CD8 (1:50; DCS diagnostics CI101C01; C8/144B) combined with rabbit anti-KLRG1 (1:20; R&D Systems MAB70293; 2388C), mouse anti-CD107a (1:500; BioLegend 328602; H4A3) and mouse anti-Granzyme B (1:100; SB 10345; 2F5F2D10). Depending on the species of the primary antibody, goat anti-mouse or goat anti-rabbit Alexa Fluor 488 (1:1000; Invitrogen A-11001 and A-11008) and goat anti-mouse or goat anti-rabbit Alexa Fluor 568 (1:1000; Invitrogen A-11004 and A-11011) were used for visualization. Lymphocytes within both SN of midbrains were counted.

2.3. Animals and stereotaxic surgery

275 male wild type (wt), 66 Recombination-activating gene 1 ($RAG\text{-}1^{-/-}$), 8 $CD4^-/CD8^+$, 14 $CD4^+/CD8^-$ and 9 $JHD^{-/-}$ ($CD4^+/CD8^+$) mice, all on the C57BL/6 background, were obtained from the animal facility of the University Hospital of Würzburg and maintained in a specific pathogen-free environment under standard conditions. Twelve weeks old mice were unilaterally injected in the right SN (Bregma: AP −3.1 mm; ML −1.4 mm; DV −4.2 mm) with 2 μl of haSyn (97 wt, 56 $RAG\text{-}1^{-/-}$) or EV (87 wt, 10 $RAG\text{-}1^{-/-}$) vector (5.16×10^{12} genomic particles (gp)/ml) as described (Ip et al., 2017). AAV were obtained from Genedetect®. Equal number of genomic particles in EV and haSyn AAV was controlled by the manufacturer. The Regierung von Unterfranken Würzburg approved all animal experiments.

2.4. Immunohistochemical stainings and cell quantification of mouse brain

Immunohistochemical stainings of mouse tissue for $CD4^+$, $CD8^+$, $B220^+$, $CD11b^+$, and TH^+ profiles were performed using 10 μm fresh coronal cryo-sections of the SN and striatum. 40 μm PFA-fixed cryosections were processed for unbiased stereology (TH) covering the whole SN. After acetone (for lymphocytes) or 4% PFA fixation (for $CD11b^+$ and TH^+), sections were incubated with either rat anti-mouse CD4 (1:1000, Serotec, cat # MCA1767), rat anti-mouse CD8 (1:500, Serotec, cat # MCA609G), rat anti-mouse CD11b (1:100, Serotec, cat # MCA74G), rat anti-mouse B220 (1:100, BD Pharmingen, cat # 550286)

or rabbit anti-mouse TH (1:1000, Abcam, cat # 112) antibodies followed by biotinylated rabbit anti-rat and goat anti-rabbit secondary antibodies (Vector Labs, cat # BA-4001 and BA-1000). Development was done using (DAB)-HCl-peroxidase (Vector Labs) and stained for TH as described.

T cells and microglia were quantified at a magnification of 200x in the region of the SN and striatum as depicted by consecutive sections stained for TH on a BH2 light microscope (Olympus). Estimation of the number of dopaminergic neurons in the SNpc and SNpr was done by unbiased stereology using the Stereo Investigator software package (v11.07, MicroBrightField Biosciences) and a BX53 microscope (Olympus, 100x/1.25 numerical aperture). Seven sections per animal covering the SN were included in quantification, separated by 160 μm (1/4 series) with grid size 110 × 110 μm, counting frame 50 × 50 μm, 2 μm guard zone, Gundersen coefficient of error for m = 1 less than or equal to 0.1. The optical density (OD) of TH^+ fibers was measured in the striatum using NIH ImageJ (v1.5). OD values were calculated as a ratio of the difference between right and left striatal OD and the unstained corpus callosum. Three striata slices per mouse were analyzed.

2.5. Double immunofluorescence for viral proteins $(VP)^+$ and tyrosine hydroxylase $(TH)^+$ dopaminergic neurons in mouse SN sections

After acetone fixation, 10 μm fresh coronal cryo-sections from mouse SN were blocked with either 5% BSA (for CD4/CD8 stainings) or 5%BSA and 10%NGS (for AAV-VP1-3 stainings) for one hour. Following blocking, sections were incubated overnight at 4° with rabbit anti-mouse TH (1:500, Abcam, cat # 112) combined with either mouse anti-AAV-VP1-3 (1:500, antibodies-online #ABIN1824130) or rabbit anti-mouse Laminin (1:50, Abcam, cat # ab11575) in combination with either rat anti-mouse CD4 (1:1000, Serotec, cat # MCA1767), rat anti-mouse CD8 (1:500, Serotec, cat # MCA609G). These proteins were then visualized using goat anti rabbit Cy3 (1:300, Dianova #111 165 144), goat anti mouse Alexa Fluor 488 (1:300, Dianova #111 595 160), and goat anti-rat Alexa Fluor 647 (1:300, Abcam ab150167). All antibodies were diluted in 1%BSA (for CD4/CD8 stainings) or 1%BSA and 1%NGS (for AAV-VP1-3 stainings).

2.6. RNA-sequencing

10–12 week old mice were injected with an AAV1/2 virus with or without haSyn into SN (n = 5 for each group). 16 weeks later, SN and striatum were microdissected, incubated for 30 min at 37 °C and 650 rpm in 1 ml HBSS with 5 mg Collagenase NB4 and 0.1 mg DnaseI followed by the generation of cell suspensions in HBSS with a 70 μm cell strainer. Cells were centrifuged at 240 g and 18 °C for 5 min. The pellet was resuspended in 30% Percoll/PBS, layered on top of a 70% Percoll/PBS gradient, and centrifuged at 650 g and 18 °C for 30 min. Immune cells were isolated at the 70/30 interphase and RNA isolation was performed with the RNeasy micro kit (Qiagen) according to manufacturer's instructions. Sequencing libraries were prepared from 0.5 ng of total RNA using the SMARTer Stranded Total RNA-Seq Kit v2 (Takara) with 4 min RNA fragmentation at 94 °C, 5 cycles of PCR for cDNA library pre-amplification and 15 cycles of PCR amplification after recombinant deoxyribonucleic acid (rDNA) depletion. The size distribution of barcoded DNA libraries was estimated ~ 430 bp by electrophoresis on Agilent High Sensitivity Bioanalyzer microfluidic chips. Sequencing of pooled libraries, spiked with 1% PhiX control library, was performed at ~ 35 million reads/sample in single-end mode with 75 nt read length on the NextSeq 500 platform (Illumina) with the High Output Kit v2.5. Demultiplexed FASTQ files were generated with bcl2fastq2 v2.20.0.422 (Illumina). To assure high sequence quality, Illumina reads were quality- and adapter-trimmed via Cutadapt version 2.5 using a cut-off Phred score of 20 in NextSeq mode. Reads without any remaining bases were discarded (command line parameters: –nextseq-trim = 20 -m 1 -a NNNAGATCGGAAGAGCACACGTCTGAACTCCAGTCAC -O 6). Reads were subsequently mapped to the mouse genome (GRCm38.p6 primary assembly and mitochondrion) and the cDNA sequence of human α-synuclein encoding SNCA A53T using STAR v2.7.2b (Dobin et al., 2013). Read counts on exon level summarized for each gene (RefSeq annotation) were generated using featureCounts v1.6.4 (Liao et al., 2014) from the Subread package. Multi-mapping and multi-overlapping reads were counted strand-specifically and reversely stranded with a fractional count for each alignment and overlapping feature (command line parameters: -s 2 -t exon -M -O –fraction). The count output was utilized to identify differentially expressed genes using DESeq2 version 1.24.0 (Love et al., 2014). Read counts were normalized by DESeq2 and fold-change shrinkage was applied by setting the parameter "betaPrior = TRUE". Due to diversity of immune cell types enriched, 1262 genes exhibiting fold changes (FC) > |1.5| in expression (log2FC > |0.6|), irrespective of adjusted p-values, were considered differentially expressed.

Z-score transformation was performed on the regularized log2-transformed read counts for the 1262 genes with FC > |1.5| and these count values were utilized to generate a heatmap using the Bioconductor/R package gplots version 3.0.3. The enrichGO (gene ontology) function in the Bioconductor/R package clusterProfiler version 3.12.0 (Yu et al., 2012) was used to perform GO over-representation analysis of the 1262 genes with a log2 fold-change >| 0.6| relative to background genes. The function barplot in gplots v3.0.3 was utilized to plot the top ten over-represented GO terms with a q-value < 0.05. The function cnetplot was applied to plot a gene concept network plot of the top ten over-represented GO terms and their respective genes. Deconvolution of relative immune cell composition on mouse expression profiles based on RNA-seq data was performed with the ImmuCC algorithm (Chen et al., 2018). To ensure high similarity to SVM training data, raw FASTQ files were independently processed for this analysis according to the ImmuCC RNA-seq pipeline (https://github.com/wuaipinglab/ImmuCC/tree/master/webserver). To this aim, the following software versions were used together with the Ensembl *Mus musculus* GRCm38 version 99 genome reference and annotation: FastQC v0.11.7, Trimmomatic-0.39, STAR-2.7.2b, samtools-1.9, RseQC-3.0.1, Htseq 0.12.4. Afterwards, the resulting expression table was subjected to web server analysis (http://218.4.234.74:3200/immune/) using the SVR method for Illumina RNA-seq data.

For the 127 genes associated with the top ten over-representing GO terms, a literature review was performed to screen for associations between individual genes and their described roles in inflammation and in neuroinflammatory diseases. Being aware that a tabular assignment of pro- vs. anti-inflammatory functions, associated cell types and possible links to neuroinflammation or PD requires considerable simplification, we sought to extract key information from the available literature. Enrichment of target genes for specific transcription factors was analyzed by using the Enrichr Online Tool https://amp.pharm.mssm.edu/Enrichr/ (Chen et al., 2013; Kuleshov et al., 2016). The 842 upregulated and, respectively, the 420 downregulated genes were loaded into Enrichr and the ENCODE and CHEA Consensus transcription factors from ChIP-X was utilized to identify the transcription factors with targets that were upregulated in the immune cells of the PD mice. Transcription Factors were sorted by p-value Ranking. The output from this analysis is provided as a supplementary table (supplementary Excel file sheet DESeq output for all genes). Sequencing data are available at GEO (http://www.ncbi.nlm.nih.gov/geo) under the accession number GSE148784.

2.7. Fluorescence-activated cell sorting (FACS) and cytokine assay

Brains, cervical lymph nodes and spleens were cut into pieces, digested with DNase I and collagenase NB4 for 30 min at 37 °C, homogenized put through a cell 70 μm strainer and centrifuged (1500 rpm) for 5 min at RT. The pellet was resuspended with 70% Percoll, overlaid with 30% Percoll and centrifuged for 30 min RT at 2000 rpm. Extracted

cells (bulk leukocytes) were stained with conjugated antibodies from BioLegend for 30 min at 4 °C: CD4-AF647 (AlexaFluor 647), CD8-PerCP-Cy5.5 (Peridin chlorophyll protein-Cyanine 5.5), and CD69-AF488. $2x10^5$ cells from brain, cervical lymph nodes, or spleen were plated in a 96-well U-bottom plate and re-stimulated with phorbol 12-myristate 13-acetate (PMA) (0.1 μg/ml, Sigma-Aldrich) and ionomycin (1 μg/ml, Sigma-Aldrich) for 4 h. Supernatants were collected, cytokine detection for IL-2, IL-4, IL-17A, and IFN-γ was carried out using LEGENDPlex™ Multi-Analyte flow assay kit from BioLegend. Data were acquired on a FACSCalibur™ (Becton Dickinson) and analyzed using FlowJo software (FLOWJO, LLC).

2.8. Behavioral tests

Behavioral studies (rotarod, cylinder test) were carried out serially on mice starting with pre-operative baseline testing and follow-up analyses until week nine after surgery.

2.8.1. Accelerating rotarod

Mice were initially trained for two days prior to pre-operative measurements. They were placed on a rotarod (RotaRod Advanced, TSE-systems) with an accelerating speed from 5 rpm to a maximum of 50 rpm for the duration of 300 s. Each day of training consisted of five runs of 300 s each. Pre-operative measurements were recorded on the third day after the two-day training session. All measurements after the two-day training consisted of five runs lasting 300 s each. Post-operative measurements were done in the 4th and 8th weeks. Latency times until mice fell off the rotarod were automatically recorded. Data are shown as latencies of 4th and 8th week relative to the pre-operative measurement for each mouse.

2.8.2. Cylinder test

Spontaneous forepaw use was evaluated using the cylinder test prior, as well as five and nine weeks post AAV1/2 injection. Mice were placed in a transparent plexiglass cylinder of 12 cm diameter and 30 cm height in front of two mirrors and were video recorded for 12 min. The videos were scored by a blinded observer as previously described (Ip et al., 2017). Each rearing of mice was assessed for the number of touches of the inner surface of the cylinder with either the right (ipsilateral), the left (contralateral), or both forepaws concurrently. The data shown represent the percentage of ipsilateral forepaw (corresponding to site of injection) use, which is calculated as follows: ((ipsilateral paw + 0.5 both paws) / (ipsilateral paw + contralateral paw + both paws)) × 100. The calculated percentage shows inclination of forepaw usage as 100% = symmetric use of both forepaws; <100% = preference of the left forepaw; >100% preference of the right forepaw.

2.9. Bone marrow transplantation

Bone marrow from approximately eight-week-old donor mice (11 wt, 14 $CD4^+/CD8^-$, 8 $CD4^-/CD8^+$, and 9 $CD4^+/CD8^+$ ($JHD^{-/-}$)) was isolated and 2×10^7 cells were injected intravenously via the lateral tail vein of restrained mice in a volume of 350 μl into seven-week-old RAG-$1^{-/-}$ mice. Blood from all recipient mice was examined for T and B cell reconstitution by FACS analysis.

2.10. Striatal dopamine transporter (DAT) autoradiography

Fresh frozen tissue sections were developed in binding buffer containing 50 mM Tris, 120 mM NaCl and 5 mM KCl at room temperature (RT). Sections were placed again in the same buffer supplemented with 50 pM [125I]-RTI-121 (Perkin-Elmer, specific activity 2200 Ci/mmol) for 2 h at 25 °C. Subsequently, slides were washed in ice-cold binding buffer, rinsed in ice-cold distilled water, and dried. Slides were then juxtaposed to an autoradiographic film (Kodak) together with [125I]-microscale standards (Amersham) and left for two days at 4 °C before development. Autoradiograms were analyzed by MCID software (Image Research Inc, Ontario, Canada). Three striatal slices per mouse were used for densitometric measurement with a reference curve of c.p.m. versus OD calculated from β-emitting [14C] micro-scale standards and used to quantify the intensity of signal as nCi/g. Background intensity was subtracted from each reading and data was expressed as the mean of signal intensity for the treatment groups. Non-specific binding was defined as that observed in the presence of 100 mM GBR 12,909 (Tocris Bioscience).

2.11. Catecholamine quantification by high-performance liquid chromatography (HPLC)

Brain sections were homogenized in 200–750 μl of 0.1 M TCA (10–2 M sodium acetate, 10–4 M EDTA, 10.5% methanol). Samples were centrifuged at 10,000 g for 20 min, supernatants were collected, and the pellets were stored for protein analysis. Catecholamines were evaluated using a specific HPLC assay with an Antec Decade II (oxidation: 0.5) electrochemical detector operated at 33 °C. Supernatant samples were injected by a Water 717 + autosampler onto a Phenomenex Nucleosil (5u, 100A) C18 HPLC column (150x4.60 mm). Analytes were eluted with a mobile phase of 89.5% 0.1 M TCA, 10^{-2} M sodium acetate, 10^{-4} M EDTA, 10.5% methanol, followed by delivery of the solvent at 0.8 ml/min with a Waters 515 HPLC pump. Analytes were examined in the following order: 3,4-dihydroxyphenylacetic acid (DOPAC), dopamine (DA), homovanillic acid (HVA). Waters Empower software was used for HPLC control and data acquisition. Total protein for each sample was determined with Pierce BCA protein assay, and the amount of catecholamines was expressed as ng analyte/mg total protein.

2.12. haSyn peptides and analysis of specific T cell responses by IFN-γ ELISpot

Using NCBI protein Blast, www.syfpeithi.de (Ver. 1.0) and netMHC4.0 (http://www.cbs.dtu.dk/services/NetMHC/), the haSyn protein sequence was aligned with murine α-synuclein and screened for potential neo-antigens likely to be presented on MHC I (H-$2D^b$ and H-$2K^b$) and MHC II (I-A^b) molecules. The three highest scoring peptides for each MHC molecule (8–15 amino acids long) were synthesized in aqua basic quality by Thermo Scientific. Each peptide was used to stimulate cells from lymph nodes or spleen followed by ELISpot assay. Splenocytes from two initially non-responsive haSyn mice and two controls were cultured for 10 days in the presence of all 10 peptides (1 μg/ml each) in RPMI with 10% FCS and 20 ng/ml IL-2. Multiscreen PVDF plates (MSIPS4510, Millipore) were activated with 35% ethanol, washed with sterile PBS and coated overnight with 2 μg/ml filtered anti-mouse IFN-γ antibody (AN18, Mabtech) at 4 °C. Isolated single cell suspensions from cervical lymph nodes and spleen were plated with or without 5 μg/ml synthetic peptide in IMDM with 7.5% FCS. IFN-γ spots were then detected with 2 μg/ml biotinylated anti-mouse IFN-γ antibody (R4-6A2, Mabtech), followed by horseradish peroxidase-conjugated streptavidin (Cell Signaling) in PBS-T supplemented with 0.05% BSA. The assay was developed with filtered "ready to use" TMB substrate (Mabtech) and analyzed using an Immunopost S6 Core Analyzer (Cellular Technology Limited). Spot analysis was performed using basic count for single color gated size above 0.01 mm^2 and normalized to non-peptide control.

2.13. Primary neuronal cell culture preparation

Primary hippocampal neurons were prepared from wt mice on embryonic day 18 of development. Hippocampi were collected in Hank's buffered saline solution (Sigma) and trypsinized with 2.5% trypsin at 37 °C for 20 min. Trypsinization was stopped with 200 μl of trypsin inhibitor, and tissue was triturated with a 1000 μl micropipette tip. Cells were pelleted for 3 min at 1400 rpm, washed three times in Neurobasal medium (Invitrogen), and resuspended in Neurobasal medium

supplemented with 1x B27, 1x Glutamax, and 1x penicillin/streptomycin. Cells were counted and seeded in a 96-well plate that had been coated overnight with 0.1% poly-L-lysine at 4 °C. After seven days of plating, cells were transduced with either $3x10^9$ of haSyn or $3x10^9$ gp/ml of EV viral vectors. Four days after transduction, T cells (200,000) were isolated from the brains of haSyn PD mice and co-cultured with neurons (20,000) in culture for 8 h. For control experiments, bulk lymph nodes cells from wt mice were collected and suspended as described above. $2x10^6$ cells were plated in a 48-well plate in 1 ml of R10 medium and stimulated for approximately 24 h with soluble low endotoxin/azide-free (LEAF) $CD3^+/CD28^+$ (E18) antibodies at a final concentration of 2.5 μg/ml each. Cells were collected, counted, and used for experiments. The activation status of T cells (CD69 expression) was always controlled by FACS analysis prior to experiments. The experiments showed that a 10:1 ratio of bulk (including primed haSyn-specific) T cells versus cultured hippocampal neurons induced no detectable changes on the gross morphology of the hippocampal neurons (Fig. 6O). For this reason, a 10:1 T cell/neuron ratio was used throughout the experiment.

2.14. Immunocytochemistry and measurement of fluorescence intensity

Neurons were fixed with 4% PFA and blocked with 5% NGS and 0.3% Triton X100 and stained with anti-mouse microtubule-associated protein-2 (MAP2, clone AP20, 1 μg/ml, Sigma, cat # M1406) and rabbit anti-human α-synuclein (1:30,000, Sigma cat # S3062) and goat anti-mouse Alexa Fluor 488 (1:300, Dianova, cat #115–545-166), and goat-anti rabbit Cy3 (1:300, Jackson laboratories, cat # 111–165-003) secondary antibodies and DAPI counterstaining. Experiments were conducted in triplicates and each cell culture well was imaged blindly and randomly using a 20x objective on a Leica DMi8 microscope. 8-bit color images were converted to 8-bit greyscale, and pixel intensity of the MAP2 staining was measured for every condition without adjustments using ImageJ. A rectangular region-of-interest was drawn around cells to determine the area and mean fluorescence-signal intensity. Background measurements were determined adjacent to cells, and the corrected total cell fluorescence (CTCF) was calculated as integrated density – (area of selected cells × mean fluorescence of background measurements).

2.15. Statistics

Normality of each data set was investigated by the D'Agostino & Pearson omnibus normality test. Parametric methods were employed for normally distributed data, and non-parametric tests were used in the instances of non-normal distributed data or unequal variances. For analysis of striatal TH^+ optical density and stereological estimation of SN cell numbers and FACS analyses the parametric one-way ANOVA was used, followed by Tukey's multiple comparison test. For the cylinder and rotarod tests, DAT autoradiography, HPLC analyses, estimation of lymphocyte numbers, cytokine analyses, and measurement of corrected total fluorescence, non-parametric tests were implemented (Mann-Whitney test for comparison of two groups, Kruskal-Wallis test for comparison of ≥ 3 groups, followed by Dunn's multiple comparison test). Unpaired, two-tailed Student's *t* test was used for comparing the number of microglial cells between two groups. Analysis of T cell-specific responses was done by two-way ANOVA with pairwise Fisher's Least Significant Difference (LSD) test. $^*P < 0.05$, $^{**}P < 0.01$, $^{***}P < 0.001$ were considered as significant P-values.

3. Results

3.1. Neuroinflammation is found in the SN of human PD brains and in the nigrostriatal tract of haSyn PD mice

Human PD brains are characterized by significantly elevated $CD8^+$ T cell numbers within the SN. Similar, though non-significant, trends were also observed for SN $CD4^+$ T cell counts ($p = 0.057$) and for perivascular $CD4^+$ T cells ($p = 0.06$) (Fig. 1A-H). Co-expression analyses further demonstrated significant elevations of Granzyme B, KLRG1 and CD107a expression in $CD8^+$ T cells in PD samples compared to human control brains (Fig. 1I, Fig. S1). $CD68^+$ myeloid cells, consisting of resident microglia and infiltrating myelomonocytic cells, were also enriched in SN samples from PD patients (Fig. 1J-L). In the haSyn PD mouse model, neuroinflammation was confirmed by staining the nigrostriatal tract for $CD4^+$ and $CD8^+$ T cells and for $CD11b^+$ myeloid cells. Compared to empty vector (EV) control mice, haSyn PD mice showed significantly increased $CD4^+$ and $CD8^+$ T cell infiltrates within the SN (Fig. 1M-O, Q-S). B cell numbers were, in contrast, low and unaltered (Fig. S2). In the striatum, where T cell infiltration was roughly ten times lower than in the SN, $CD4^+$ but not $CD8^+$ T cell counts were significantly elevated in haSyn PD mice over controls (Fig. 1P, T). By directly comparing T cell numbers between human PD and haSyn PD mouse samples, we found ~ 20x more $CD4^+$ and ~ 10x more $CD8^+$ T cells in haSyn mice. Moreover, while most T cells observed in haSyn PD mice were found in the SN parenchyma (~80% for both T cell subpopulations), only ~ 30% of T cells in human PD samples were located in the parenchyma and ~ 70% showed perivascular localization (Fig. 1U-W, Fig. S3). $CD11b^+$ microglia and other myeloid cells were well represented in the SN and striatum, with significantly elevated cell numbers and increased surface expression in haSyn PD mice compared to EV controls (Fig. 1X-Z1). In line with the faster onset and progression of disease, the haSyn PD mouse model demonstrates a higher amount of T cell accumulation. Also, the proportion of lymphocytes in the parenchyma was higher in brains from haSyn mice than in the SN of PD patients. Still, both the nigrostriatal tract of haSyn PD mice and the SN of human PD brains were characterized by neuroinflammation.

3.2. Differentially expressed pro-inflammatory gene profile of immune cells in the brains of haSyn PD mice

To obtain broader insights into the immune activation in the haSyn PD mouse brain, we sacrificed haSyn PD and EV control mice 16 weeks after AAV1/2 injection into the SN, isolated the immune cells from the SN and striatum and performed RNA sequencing. The advanced disease time point was chosen to ensure sufficient accumulation of immune cells in this progressive and low-grade inflammatory model of PD. Moreover, as most human patients only receive the clinical diagnosis of PD once they have already suffered an estimated loss of > 50% of all dopaminergic SN neurons (Dauer and Przedborski, 2003; Lang and Lozano, 1998; Marsden, 1990; Ross et al., 2004), the late time point is also expected to enhance comparability. As expected, monocyte-like cells (likely microglia) made up the majority of the analyzed cells. Deconvolution of expression profiles (Chen et al., 2017) also confirmed the presence of other immune cell types including $CD4^+$ and $CD8^+$ T cells (Fig. 2A). We considered a Fold Change cutoff of |1.5| to screen for biological trends in the data. This approach still yielded 1262 genes that were differentially expressed in haSyn PD mice compared to EV control (Fig. S4). Pathway analysis based on Gene Ontology (GO) enrichments indicated inflammation-associated processes (Fig. 2B, supplementary excel file, GO Analysis table). Out of the 127 deregulated genes falling into these GO categories, 117 were up- and 10 downregulated (Fig. 2C). Eighty-One of the upregulated genes (69%) were described as pro-inflammatory in the UniProt database (https://www.uniprot.org/), thereby indicating a pro-inflammatory shift in the brains of haSyn PD mice (Fig. 2C, supplementary excel file, upregulated/downregulated gene tables). Cell types associated with these 127 genes included lymphocytes in general (mentioned 17 times), macrophages (45), dendritic cells (43), T cells (43), monocytes (42), granulocytes (36 including 13 neutrophils and 3 basophils), B cells (21), NK cells (16), and mast cells (11). Moreover, 32 genes (25%) had previously been implicated in neuroinflammation. PD-associated pro-inflammatory genes *Aif1*, *Casp1*,

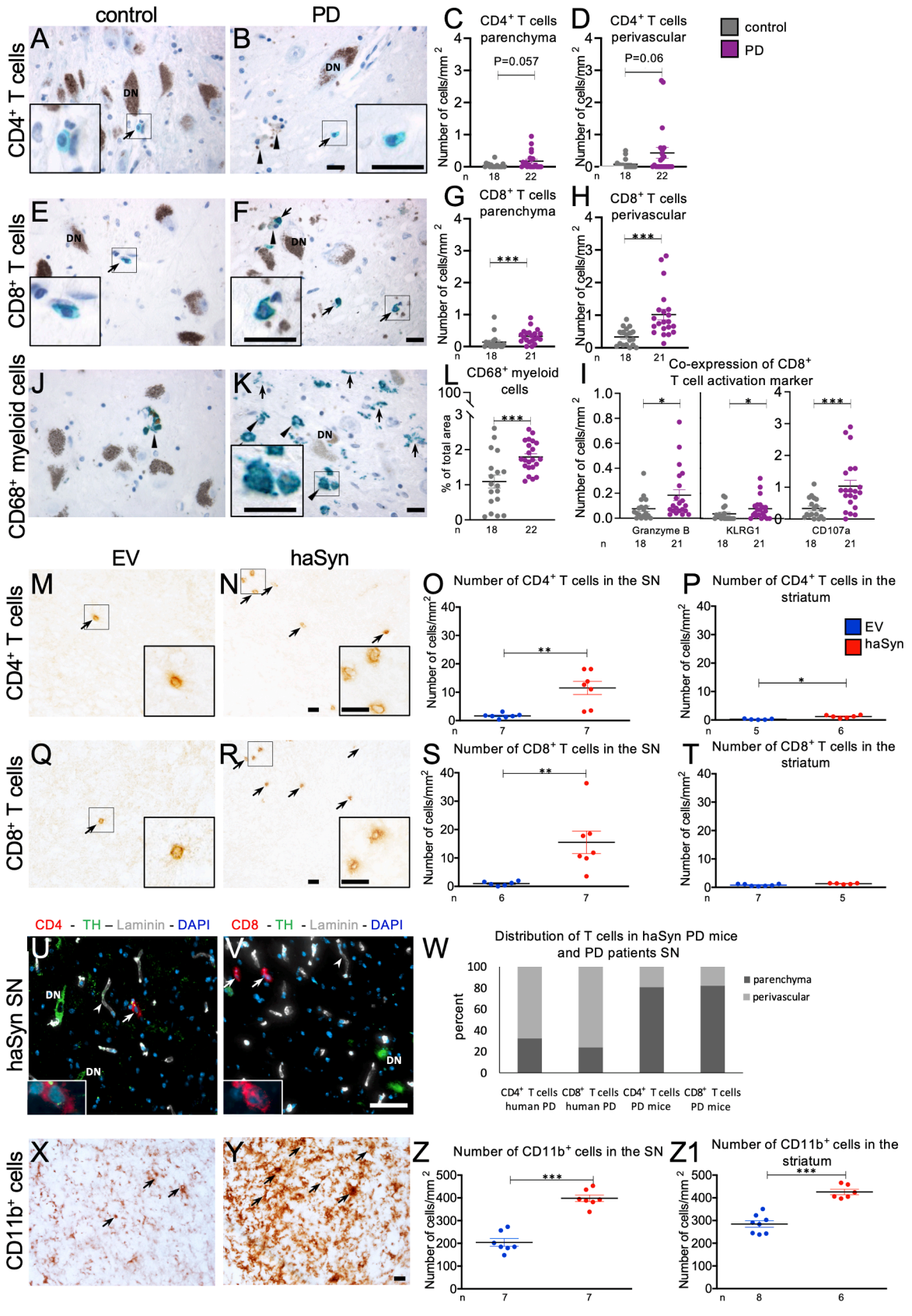

(caption on next page)

Fig. 1. Human PD brains and haSyn PD mice demonstrate T cell and myeloid cell accumulations. A, B, E, F, J, K Representative images of human control (A, E, J) and PD patients (B, F, K) brain autopsies stained and counted for $CD4^+$ (A-D) and $CD8^+$ (E-H) T cells (arrows) and $CD68^+$ myeloid cells (J-L) in the SN. Co-expression of $CD8^+$ T cells with activation marker Granzyme B, KLRG1 and CD107a (I). Macrophages in B, F, J and K depicted by arrowheads, arrows in K point at processes of microglia, dopaminergic neurons marked as DN (A, B, E, F, K). M–T, Immunohistochemical stainings and quantification for $CD4^+$ (M–P) and $CD8^+$ (Q-T) T cells in the SN and striatum of EV vector (EV) and haSyn vector (haSyn) injected mice, ten weeks after AAV injection. U, V, Triple-immunofluorescence images from haSyn mouse SN stained for $CD4^+$ (U) or $CD8^+$ T cells (V), TH for dopaminergic neurons and Laminin as vessel marker. Relative distribution of T cells regarding the proximity to vessels in haSyn PD mice and human PD SN (W). X-Z1, Images (X, Y) from $CD11b^+$ immunostained myeloid cells and cell counts (Z-Z1) from EV control (Z) and haSyn PD mice (Z1). Data shown as mean ± SEM. n (A-L) = number of human SN; n (M–Z1) = number of biologically independent animals. Statistical analysis by one-tailed Mann-Whitney test for human samples, by unpaired, two-tailed Student's *t* test: SN $t(12) = 8.804$, $P < 0.0001$; striatum: $t(12) = 7.167$, *$P < 0.05$, **$P < 0.01$, ***$P < 0.001$. Scale bars: B, F, K, V 50 μm each, N, R, Y 20 μm each.

Il1b, *Jun*, *Sphk1*, *Tnf*, and *Trem2*, and anti-inflammatory *Gpnmb* and *Fcgr2b* genes were also found to be upregulated in haSyn PD mice (supplementary excel file, upregulated/downregulated gene tables). Based on the 1262 genes with $> |1.5|$ fold change, transcription factor enrichment analyses (supplementary excel file, ENCODE and ChEA3 Consensus TFs table) revealed significant upregulation of SPI1 (Padj = 0.001; 74 genes) and IRF8 (Padj = 0.002; 16 genes) which have already been linked to alterations of gene expression in human PD (Satoh et al., 2014; Su et al., 2018). Other transcription factors were not significantly enriched.

3.3. T cells in the brain of haSyn mice display an activated marker profile

Since T cell related genes were prominently altered in haSyn PD mice, we characterized T cells from these mice compared to EV controls and naïve wild type (wt) mice by FACS analysis. One, five and ten weeks after disease induction, T cell activation was assessed in brain, cervical lymph nodes, and spleen using CD69 as an activation marker. One week after injection, detection of AAV coating proteins in > 95% of dopaminergic SN neurons from both haSyn and EV mice confirmed a similar transduction efficiency in both groups (Fig. S5). At the same time point, a significant elevation of $CD8^+CD69^+$ T cells was found in brains of haSyn PD and EV mice compared to naïve wt controls. This elevation was observed until 5 weeks after AAV delivery. At ten weeks, however activated $CD4^+CD69^+$ and $CD8^+CD69^+$ T cells were significantly increased only in haSyn PD mouse brains compared to age-matched EV controls and all other groups (Fig. 3A-H). This level of T cell activation persisted and was also observed at the 16 weeks time point chosen for gene expression analysis (Fig. S6). Irrespective of the chosen time point, cervical lymph nodes from haSyn PD mice showed no induction of CD69 while the spleen of haSyn PD mice demonstrated only significantly increased activation of $CD4^+$ and $CD8^+$ T cells compared to the one weeks groups of mice (Fig. 3A-H).

3.4. T cells from peripheral lymphatic organs of haSyn PD mice express an early pro-inflammatory cytokine profile

In addition to T cell activation, we further determined cytokine release in response to PMA/ionomycin. One week after disease induction haSyn PD mice displayed a prominent elevation of IL-2 in cervical lymph nodes and spleen. This finding possibly indicates a T cell activation in peripheral organs (Fig. 3I-K). Interestingly, no significant IL-2 release was observed in T cells from brain at the early stages. A very recent report also suggests that T cells persisting in the brain undergo epigenetic adaptations induced by the transcription factor TOX which result in a partial loss of effector functions (Page et al., 2021). Responsive T cells detected at 5 weeks after infection may thus have freshly immigrated into the brain. Further cytokine analyses to indicate T cell polarization into Th1, Th2 or Th17 $CD4^+$ T helper cell subsets revealed heterogeneous results. IL-4 as a marker for Th2 immunity did not show any significant differences between haSyn PD mice and EV controls. In addition, non-significant trends towards elevated IFN-γ and IL-17 production were detectable in cervical lymph nodes (IL-17) and spleen (IFN-γ) at early time points (Fig. 3L-T). Altogether, these results support an early peripheral T cell priming event, as indicated by IL-2 release from spleen and cervical lymph node cells. Responses observed in both EV and α-synuclein-injected, but not in control mice, are likely directed against AAV antigens. Initial priming of T cells against AAV and α-synuclein antigens may also explain the ambiguous polarization of early immune responses, with traits of Th1, Th2 and Th17 signatures. However, as T cell activity in EV-infected mice subsides to control levels within weeks, T cell responses assessed at later time points are likely α-synuclein-specific.

3.5. Genetic lymphocyte deficiency alleviates motor symptoms and prevents SN dopaminergic perikarya loss without rescuing dopaminergic terminals in the striatum of haSyn PD mice

To evaluate the functional role of adaptive immune cells in nigrostriatal degeneration and ensuing deterioration of motor function, we performed rotarod performance and cylinder tests on haSyn PD mice with or without RAG-1 deficiency. RAG-1 deficient mice produce no mature lymphocytes and can therefore indicate a role for these cells in PD disease progression. While all EV control groups showed a consistent performance, haSyn PD mice displayed a significant deterioration of motor performance on the rotarod at four and, to a more pronounced extent, at eight weeks (Fig. 4A). In line with the predicted role for lymphocytes in disease progression, RAG-1 deficiency ($RAG\text{-}1^{-/-}$ haSyn) prevented this deterioration (Fig. 4A). This protection of motor symptoms was also found by cylinder tests nine weeks after disease induction (Fig. 4B). A preference for using the right forepaw, ipsilateral to the injection site of the right SN, was observed in immune-competent wt haSyn PD mice but not in EV control or $RAG\text{-}1^{-/-}$ haSyn PD animals. A comparison between the five week and the nine week time points also indicates the progressive character of this imbalance in the cylinder test. To demonstrate that the absence of lymphocytes and not genotype-related factors were the cause for the amelioration of motor symptoms, $RAG\text{-}1^{-/-}$ mice were reconstituted with lymphocytes by bone marrow transfer (Fig. 4D-E). In these immunologically reconstituted (wt BM $RAG\text{-}1^{-/-}$ haSyn PD) mice, infiltration of T cells into the nigrostriatal system was comparable to wt haSyn PD mice (Fig. 4C) and associated with a significant deterioration of motor performance compared to their $RAG\text{-}1^{-/-}$ haSyn counterparts. In line with the behavioral tests, quantification of dopaminergic SN neurons ten weeks after disease induction revealed a substantial cell loss in wt haSyn PD mice that was hardly observed in $RAG\text{-}1^{-/-}$ haSyn PD mice. Reconstitution of lymphocytes in $RAG\text{-}1^{-/-}$ haSyn PD mice (wt BM $RAG\text{-}1^{-/-}$ haSyn PD) restored the pathology (Fig. 4F, G). These data clearly demonstrate the pathogenic role of lymphocytes in SN dopaminergic neurodegeneration. Interestingly, optical density measurement of TH^+ fibers and autoradiography-based dopamine transporter (DAT) binding analyses, performed to assess the striatal innervation with dopaminergic terminals, revealed that the loss of dopaminergic terminals was lymphocyte-independent. Ten weeks after disease induction, all groups of mice injected with the pathogenic haSyn vector (wt, $RAG\text{-}1^{-/-}$, wt BM $RAG\text{-}1^{-/-}$) showed reduced TH^+ optical density and striatal DAT binding on the injected side, whereas no apparent loss of dopaminergic terminals was visible in EV injected wt and $RAG\text{-}1^{-/-}$ mice (Fig. 4H-J). Striatal dopamine levels ipsilateral to the haSyn vector injection were similarly reduced in wt, $RAG\text{-}1^{-/-}$ mice, and in wt bone marrow reconstituted $RAG\text{-}1^{-/-}$ mice (Fig. 4K). Still, the

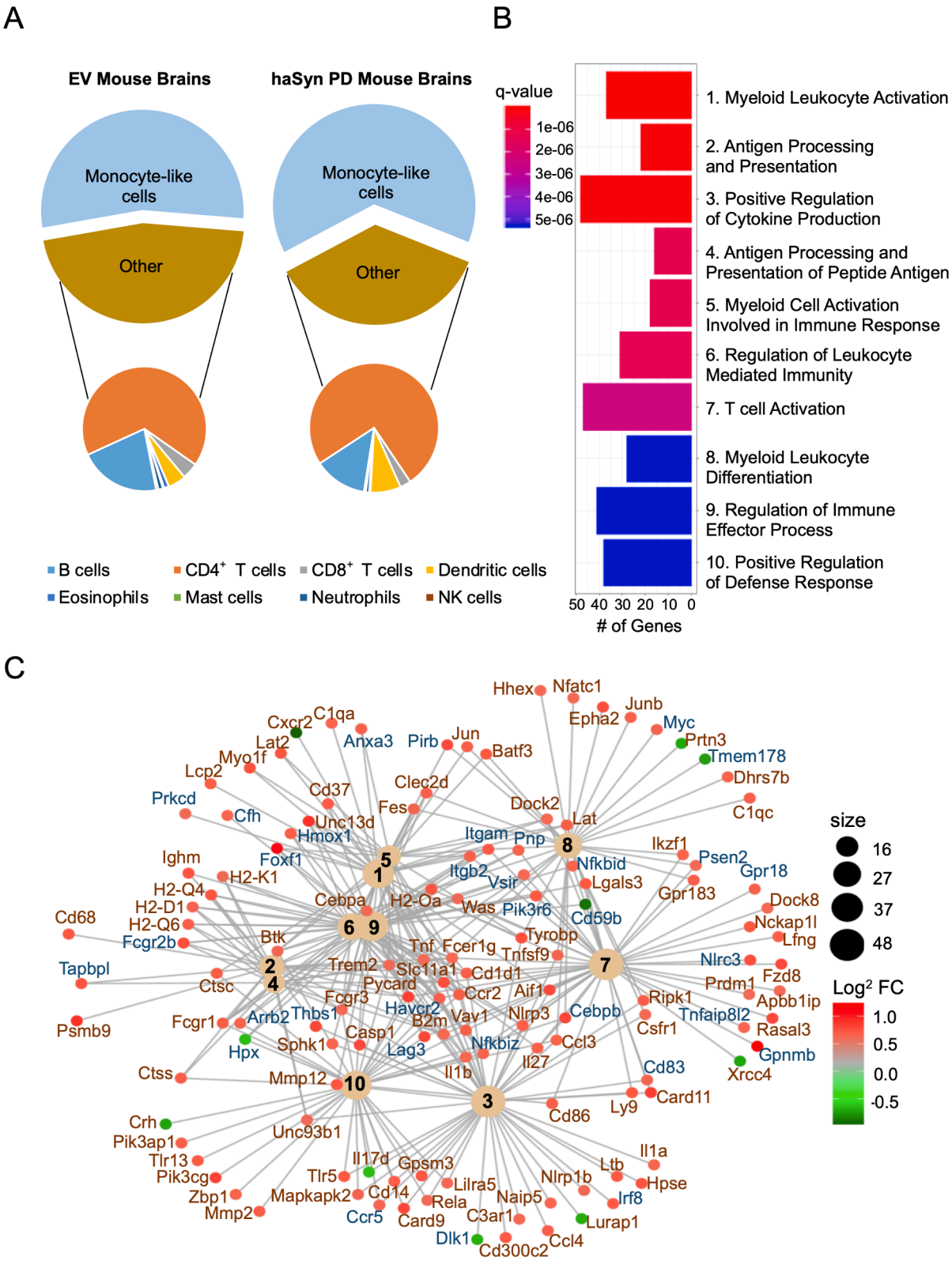

Fig. 2. Transcriptome analysis of brain immune cells reveals an inflammatory profile in haSyn PD mice. A, Pie Charts depicting the relative distribution of the various immune cell types from EV (left) and haSyn PD (right) mouse brains after discontinuous Percoll gradient to enrich for immune cells in the SN and striatum. Data represent the average of five mice each. B, Bar plot depicting the top enriched GO terms from the genes with a FC > |1.5| (log2FC > |0.6|) in haSyn PD mice compared to EV control. X-axis represents the number of genes and colors are depicting the q-values for the GO term enrichment. C, Network map of the top 10 upregulated GO terms from B and the genes associated with these GO terms. Genes are color-coded for fold change with green dots representing down-regulation and red dots representing up-regulation, with brown letters representing described pro-inflammatory and blue letters representing anti-inflammatory roles. Tan circles represent the individual GO terms, numbered as in B. (For interpretation of the references to color in this figure legend, the reader is referred to the web version of this article.)

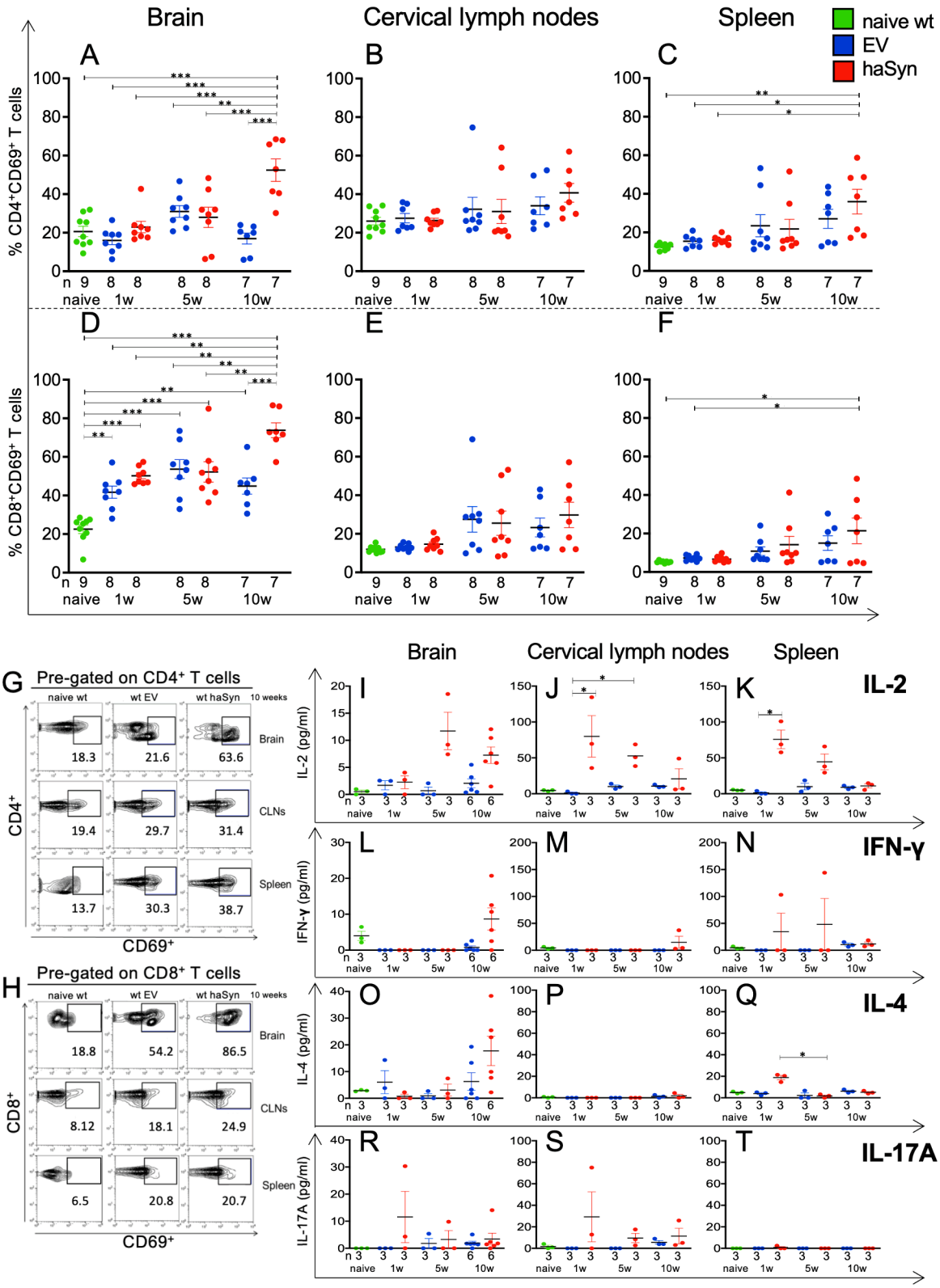

Fig. 3. Activation of T cells and early elevation of cytokines in haSyn PD mice. A-H, FACS-based staining for $CD4^+CD69^+$ or $CD8^+CD69^+$ activated T cells in haSyn PD mice compared to EV and naïve controls of brain (A, D), cervical lymph nodes (B, E), and spleen (C, F) one, five and ten weeks after AAV injection. Representative FACS results are shown for at ten weeks for $CD4^+CD69^+$ (G) and $CD8^+CD69^+$ T cells (H). I-T, Cytokine analyses from supernatants of cells derived from the indicated organs after ex vivo stimulation with PMA/ionomycin. IL-2 (I-K), IFN-γ (L-N), IL-4 (O-Q), and IL-17A (R-T) levels. Data shown as mean ± SEM. n = number of biologically independent samples, each sample for cytokine analyses consist of pools of two animals. Statistical analysis by one-way ANOVA with Tukey for FACS ($CD4^+CD69^+$ brain: $F(6, 48) = 10.64$, $P < 0.0001$; $CD4^+CD69$ spleen: $F(6, 46) = 3.594$, $P = 0.0053$. $CD8^+CD69^+$ brain: $F(6, 48) = 17.02$, $P < 0.0001$; $CD8^+CD69$ spleen: $F(6, 47) = 2.998$, $P = 0.0146$) and Kruskal-Wallis test followed by Dunn's multiple comparison test for each time point for cytokine analyses. *$P < 0.05$, **$P < 0.01$, ***$P < 0.001$.

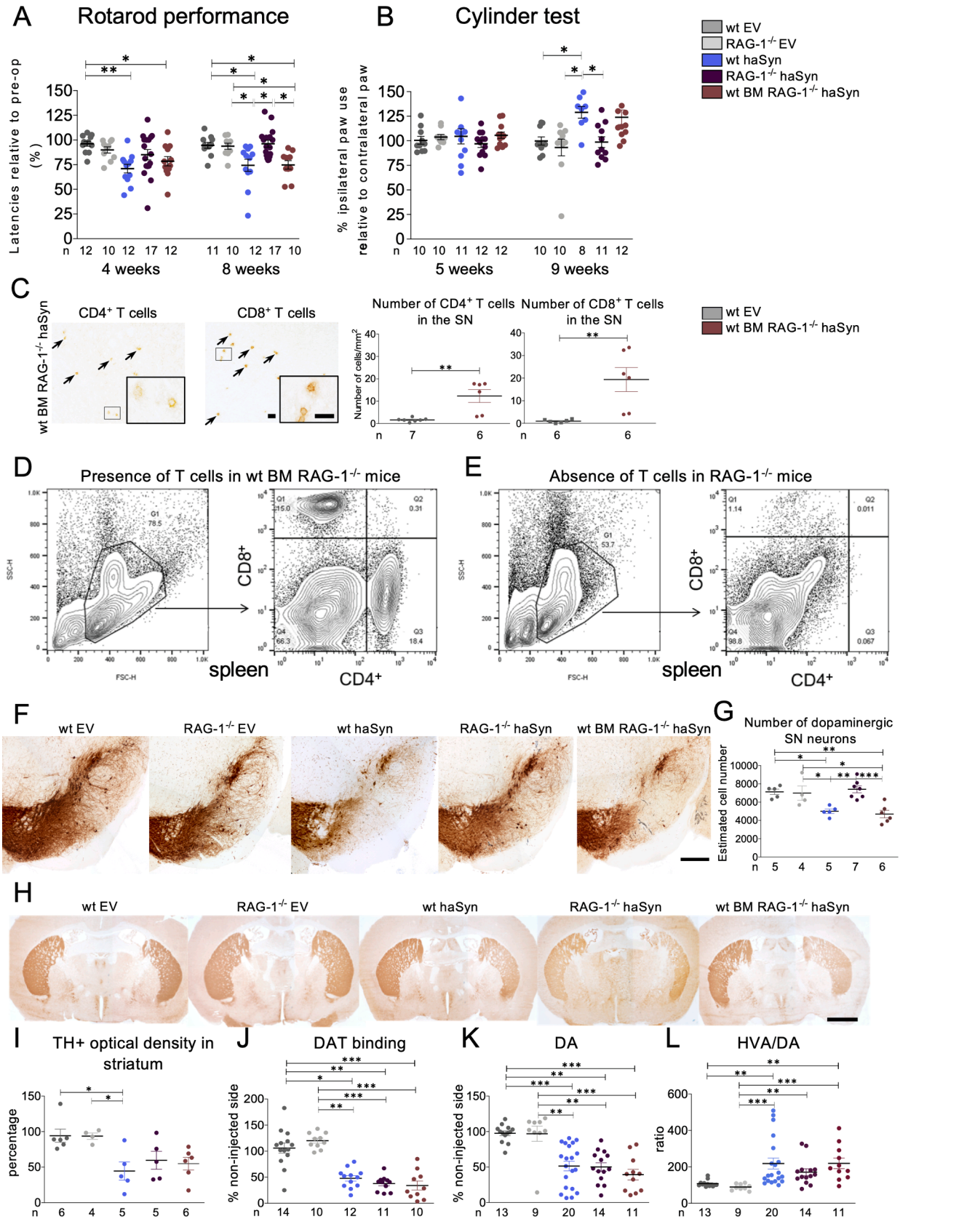

(caption on next page)

Fig. 4. Lymphocytes contribute to nigrostriatal dopaminergic degeneration in the haSyn PD mouse model. A, B, Data from rotarod performance and cylinder test of EV vector-injected wt and RAG-1$^{-/-}$ control mice, immune-competent haSyn PD mice (wt aSyn), RAG-1$^{-/-}$ haSyn mice and bone marrow reconstituted RAG-1-/- haSyn PD mice (wt BM RAG-1$^{-/-}$ haSyn). C-E, For each animal, successful reconstitution of T cells by wt bone marrow transfer into RAG1$^{-/-}$ mice was demonstrated by the presence of T cells in FACS analysis of the spleen and by infiltration of the SN with CD4^{+} and CD8^{+} T cells. In compliance with rules for the reduction of animal use in research, the wt EV data for C are identical to the ones presented in Fig. 1O, S. F-G, Representative images of TH^{+} dopaminergic neurons in the SN of the indicated groups of mice (F) and estimated cell number of SN neurons by unbiased stereology (G). H-I, Representative images from the indicated groups of mice showing the dorsolateral striatum after TH^{+} immunostaining. Optical density measurements (I). J, DAT autoradiography in the striatum of the same groups of mice. K-L, Analyses of striatal dopamine levels and HVA/DA ratio. All data are shown as mean ± SEM. n = number of biologically independent animals. Statistical analysis for A, B, J-L: Kruskal-Wallis test followed by Dunn's multiple comparison test. For C: Mann-Whitney test, for G, I: one-way ANOVA followed by Tukey's multiple comparison test: SN: $F(4, 22) = 9.779$, $P = 0.0001$; Striatum: $F(4, 21) = 4.901$, $P = 0.0060$. *P < 0.05, **P < 0.01, ***P < 0.001. Scale bars: C: 20 μm; F: 200 μm; H: 1000 μm.

homovanilic acid (HVA) to dopamine ratio revealed a significantly higher dopamine turnover in wt haSyn PD mice compared to wt and RAG-1$^{-/-}$ EV-injected controls. RAG-1 deficiency resulted in a slight reduction of the HVA/dopamine ratio after haSyn vector injection, while lymphocyte reconstitution with wt bone marrow enhanced the HVA/dopamine ratio again (Fig. 4L). Thus, lymphocyte deficiency can completely reverse behavioral deficits and most histological alterations, whereas lymphocyte reconstitution sets back the phenotype to wt impaired haSyn PD mice. Brain-infiltrating lymphocytes hence play a critical functional role in neurodegeneration in the haSyn PD model.

3.6. CD4^{+} and CD8^{+} T cells both induce relevant damage to dopaminergic SN neurons

To further define the lymphocyte subpopulation(s) responsible for the observed dopaminergic SN cell loss in immune-competent haSyn PD mice, we reconstituted RAG-1$^{-/-}$ mice with bone marrow from mice lacking either CD4^{+} (CD4^{-}/CD8^{+}) or CD8^{+} (CD4^{+}/CD8^{-}) T cells or B cells (CD4^{+}/CD8^{+}). Successful bone marrow transfer was controlled by FACS analysis of blood and spleen lymphocytes (Fig. 5A-C). Ten weeks after virus delivery, dopaminergic SN neurons were reduced in haSyn-injected RAG-1$^{-/-}$ mice that received CD4^{+}/CD8^{-}, CD4^{-}/CD8^{+} or JHD$^{-/-}$ bone marrow compared to EV control RAG-1$^{-/-}$ mice (Fig. 5D, E). Analysis of striatal dopaminergic fiber innervation again demonstrated a loss of striatal fibers in all mice injected with the haSyn vector, and a

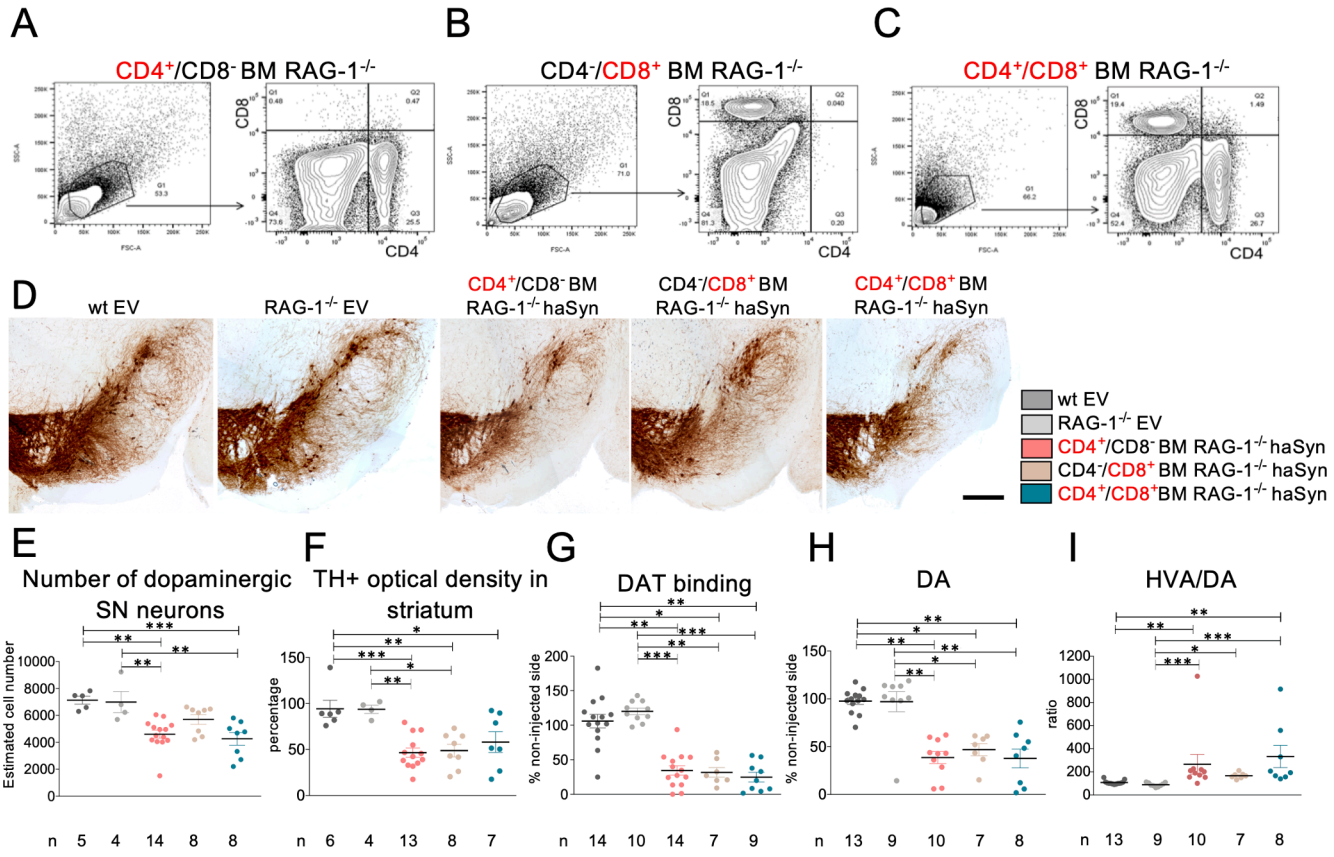

Fig. 5. CD4^{+} and CD8^{+} T cells are both detrimental in the haSyn PD mouse model. A-C, Representative FACS analyses of mouse spleens from RAG-1$^{-/-}$ mice after successful transplantation with either CD4^{+}/CD8^{-}, CD4^{-}/CD8^{+}, or CD4^{+}/CD8^{+} bone marrow showing reconstituted CD4^{+} or CD8^{+}, or CD4^{+}+CD8^{+} T cells, respectively. B cells, which are also lacking in RAG-1$^{-/-}$ mice, were not reconstituted in this assay. (D-E) TH immunostained SN images showing dopaminergic neurons from EV vector-injected controls (wt EV, RAG-1$^{-/-}$ EV) and from the three T cell reconstituted mouse groups injected with haSyn as indicated (D). Number of dopaminergic SN neurons (E). F-G, Optical density measurements (F) and DAT binding in striatum (G). H-I, Striatal dopamine levels and HVA/DA ratio. Data shown as mean ± SEM. n = number of biologically independent animals. In compliance with rules for the reduction of animal use in research, the wt EV and RAG-1$^{-/-}$ EV data for E-I were identical to the ones presented in Fig. 4G, I-L. Statistical analysis for E and F: one-way ANOVA followed by Tukey's multiple comparison test: E: $F(4,34) = 8.485$, $P < 0.0001$; F: $F(4, 33) = 8.392$, $P < 0.0001$. For G-I: Kruskal-Wallis test followed by Dunn's multiple comparison test. *P < 0.05, **P < 0.01, ***P < 0.001. Scale bar: D: 200 μm.

A

MDVFMKGLSK AKEGVVAAAE KTKQGVAEAA GKTKEGVLYV GSKTKEGVVH
GVTTVAEKTK EQVTNVGGAV VTGVTAVAQK TVEGAGSIAA ATGFVKKDQL
GKNEEGAPQE GILEDMPVDP DNEAYEMP(L)SE EGYQDYEPEA

B

hu_aSyn68-76	G A V V T G V T A	H-2D^b	MHC I
hu_aSyn68-78	G A V V T G V T A V A	H-2D^b	MHC I
hu_aSyn80-94	K T V E G A G S I A A A T G F	I-A^b	MHC II
hu_aSyn92-100	T G F V K K D Q L	H-2K^b	MHC I
hu_aSyn99-107	Q L G K N E E G A	H-2D^b	MHC I

hu_aSyn100-107	L G K N E E G A	H-2K^b	MHC I
hu_aSyn100-114	L G K N E E G A P Q E G I L E	I-A^b	MHC II
hu_aSyn120-134	P D N E A Y E M P S E E G Y Q	I-A^b	MHC II
hu_aSyn121-128	D N E A Y E M P	H-2K^b	MHC I
hu_aSyn121-128 P128L	D N E A Y E M L	H-2K^b	MHC I

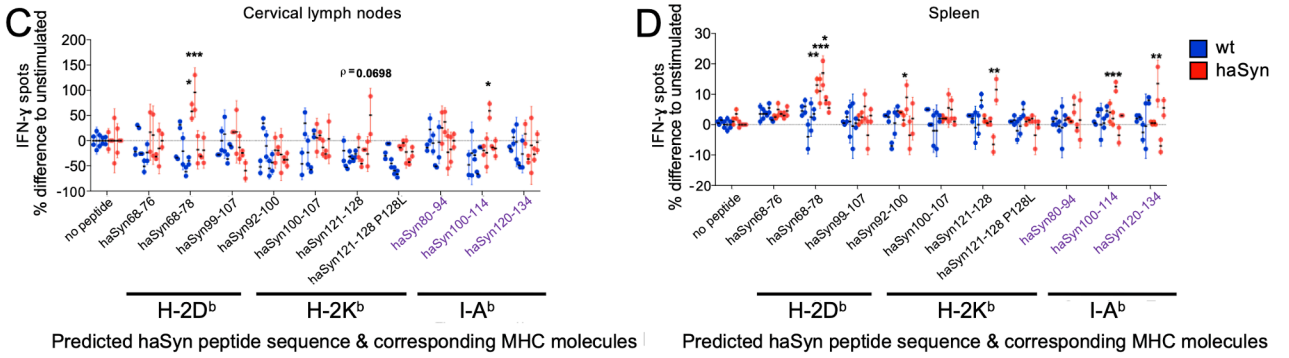

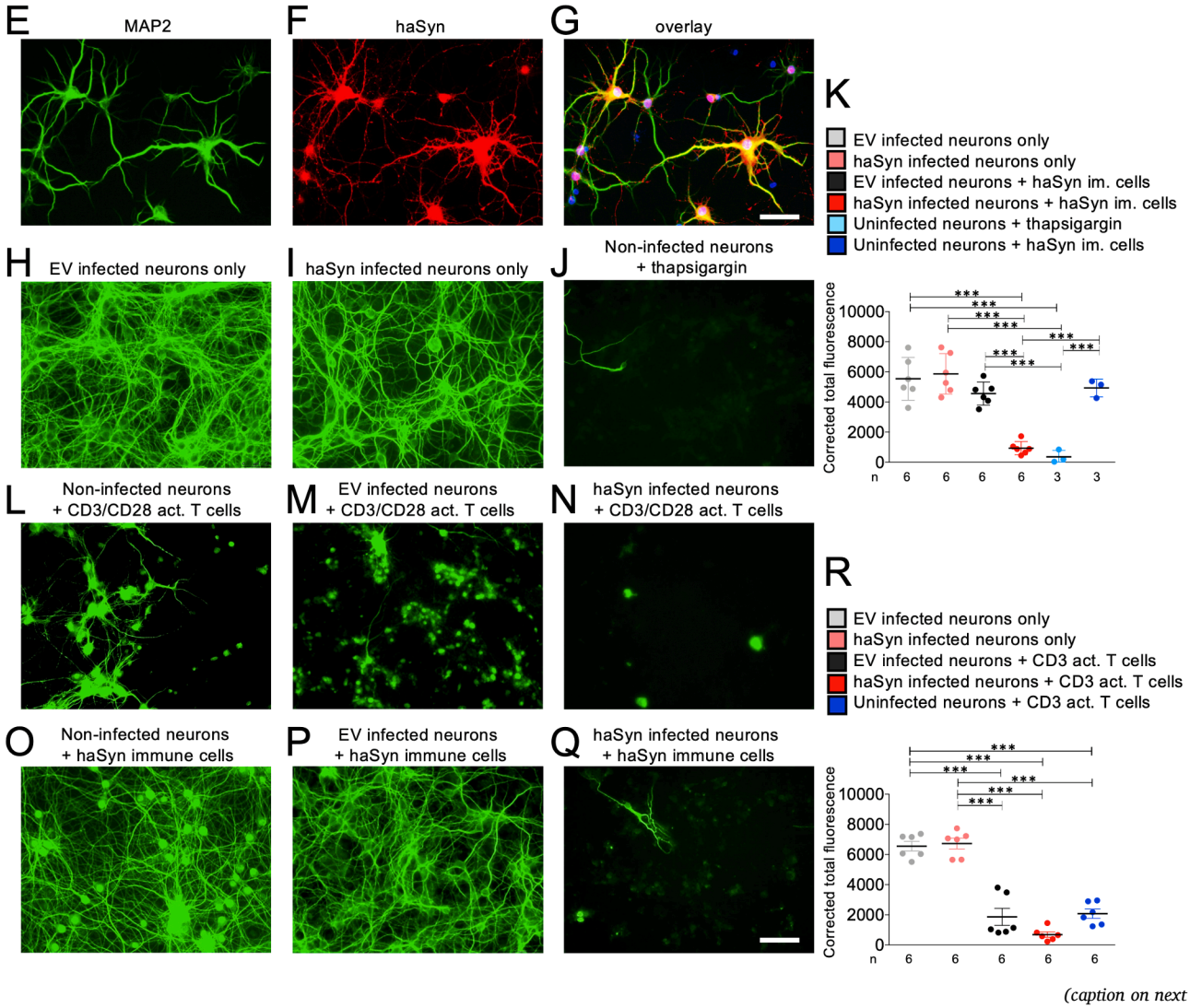

(caption on next page)

Fig. 6. Causative link between α-synuclein-specific T cell responses and immune system-elicited neurodegeneration. A, Amino acid sequence of mutated human A53T-haSyn. The mutation at position 53 is highlighted in red. Amino acids that differ between mouse and human aSyn are shown in blue. The P128L modification is shown in orange brackets. B, Ten peptides predicted to bind to MHC I H-2 molecules K^b, D^b, and MHC II molecule I-A^b generated from the human haSyn sequence are shown with amino acid sequence and position. C, Results from IFN-γ ELISpot analysis after stimulation of mononuclear cells containing $CD4^+$, $CD8^+$ T cells and myeloid cells from cervical lymph nodes of haSyn PD (red) and control mice (blue) with the predicted peptides, ten weeks after EV or A53T vector injection. D, Leukocytes from spleens of haSyn PD and control mice were incubated with all ten predicted haSyn peptides for ten days. Values are shown as mean ± SEM. n = 5 biologically-independent animals for each group. E-G, Image showing immunofluorescence stainings of MAP2 (E, green) and haSyn (F, red) in hippocampal neurons expressing haSyn after viral infection. Overlay with DAPI (G). H-J, L-N, O-Q, Primary neuron cultures in 96-well plates that were infected with EV vector (H, M, P), haSyn vector (I, N, Q), or remained non-infected (J, L, O). Co-cultures with mononuclear cells including T cells from haSyn brains, extracted ten weeks after AAV delivery (O-Q), CD3/CD28-activated T cells (L-N), or thapsigargin (J). K, R, Measurement of MAP2 fluorescence intensity shown as mean ± SEM. n = number of biologically independent cell cultures for each experiment. Statistical analysis for C and **D** by two-way ANOVA with pairwise Fisher's LSD test (C: $F(10, 110) = 2.629$, $P = 0.0066$; D: $F(10, 110) = 4.099$, $P < 0.0001$), for **K, R** by Kruskal-Wallis test followed by Dunn's multiple comparison test. *P < 0.05, **P < 0.01, ***P < 0.001. Scale bars: 50 μm each. (For interpretation of the references to color in this figure legend, the reader is referred to the web version of this article.)

corresponding dopaminergic terminal loss as reflected by reduced striatal TH^+ fiber innervation and DAT binding (Fig. 5F, G). Reduction of striatal dopamine and increase of dopamine turnover was observed in all three groups of mice after haSyn vector injection (Fig. 5H, I). In summary, these data indicate that both $CD4^+$ and $CD8^+$ T cells but not B cells are detrimental to dopaminergic SN neurons.

3.7. haSyn peptides elicit antigen-specific responses

Having demonstrated the pathogenic relevance of T cells in the haSyn PD mouse model, we screened for antigen-specific T cell responses against haSyn epitopes. Ten weeks after AAV injection, mononuclear cells including bulk $CD4^+$ and $CD8^+$ T cells were extracted from cervical lymph nodes or from spleens of haSyn vector-injected mice, before being stimulated with haSyn-derived peptides and tested for IFN-γ production by ELISpot assays. Peptide antigen candidates from the mutated human haSyn sequence (Fig. 6A) were selected based on neoantigenicity (due to species difference), on predicted affinity and on the likelihood of being presented by murine MHC I molecules H-2 K^b and H-2D^b and by the MHC II molecule I-A^b (Fig. 6B). The haSyn peptide 121–128 was further modified (P128L) to increase predicted affinity to H-2 K^b. Out of ten predicted peptides, haSyn68-78 and haSyn100-114 elicited increased IFN-γ production in ELISpot assays with T cells isolated from cervical lymph nodes of 3/5 haSyn PD mice (Fig. 6C). Cells from control animals did not respond. To improve the signal to noise ratio, antigen-specific T cells were cultured for 10 days in the presence of all ten peptides (+IL-2). After resting, the *in vitro* expanded T cells were stimulated with individual peptides and IFN-γ production was assessed by ELISpot. Cells from the two initially non-responsive haSyn PD mice now also displayed significantly increased IFN-γ production in response to haSyn68-78 peptide (Fig. 6D). In addition, elevated IFN-γ levels were observed in haSyn PD mice for haSyn92-100, 121–128, 100–114 and 120–134 (Fig. 6D). Thus, T cells from peripheral lymphatic organs of all tested haSyn PD mice showed antigen-specific T cell responses to at least one peptide of the mutated human haSyn protein, with a preference for haSyn68-78. haSyn antigen-specific T cells can thus be detected in cervical lymph nodes and, albeit at lower frequencies, in spleens from haSyn PD mice. Since ELISpot analyses from brain mononuclear cells at ten weeks of disease did not yield clear results, we repeated the experiment with mice at an earlier disease stage, two weeks after haSyn vector injection This revealed a significantly increased IFN-γ production, again in response to the haSyn68-78 and haSyn120-134 peptides. No such responses were found in EV injected mice (Fig. S7). Interestingly, the number of haSyn-transduced TH^+ SN neurons was higher at two weeks than at ten weeks after AAV delivery, mostly because of the degeneration of TH^+ neurons (Fig. S8). This finding could therefore explain the differences in haSyn-responsiveness of T cells comparing these two time points. Taken together, our results indicate a two-phasic disease course in haSyn PD mice with an early phase (1–5 weeks) characterized by peripheral immune activation (IL-2 increase in cervical lymph nodes and spleen) and haSyn-specific-immunoreactivity of brain T cells and a late phase (10–16 weeks) with pronounced neuroinflammation and T cell activation ($CD69^+$) in the brain.

3.8. Mononuclear cells isolated from haSyn-expressing brains specifically induce damage to haSyn-expressing neurons

To clarify whether murine T cells that specifically respond to human haSyn peptides can actively induce haSyn-specific damage to neurons, primary mouse hippocampal neurons were infected with haSyn or control vector. Four days after infection, all haSyn vector-infected neurons expressed haSyn (Fig. 6E-G) and displayed cell numbers and cell integrity comparable to EV infected cells, as judged by the neuronal somatodendritic marker MAP2 (Fig. 6H, I). Treatment with thapsigargin reduced MAP2 staining by > 80% (Fig. 6J, K). We then performed an *ex vivo/in vitro* study by extracting mononuclear cells (including T cells and microglia) from haSyn PD mouse brains. Unspecific activation of T cells with anti CD3/CD28 antibodies elicited massive cell loss in both naïve and vector-infected neurons (Fig. 6L-N, R), thereby confirming functionality of the isolated immune cells. Incubation of haSyn-infected neurons for eight hours with brain leukocytes from haSyn PD mice likewise resulted in massive (>80%) neuron damage (Fig. 6Q, K). In contrast, EV-infected and non-infected naïve neurons did not suffer from incubation with mononuclear cells derived from haSyn PD mouse brains (Fig. 6O, P, K). This assay thus showed that mononuclear cells from brains of haSyn PD mice induced neuronal damage in a strictly haSyn antigen-specific manner, which indicates that T cells (rather than microglia) are the critical effectors.

4. Discussion

There is increasing evidence for involvement of adaptive immunity in PD pathophysiology (Brochard et al., 2009; Lindestam Arlehamn et al., 2020; Sommer et al., 2018; Sulzer et al., 2017; Williams et al., 2021). Knowing α-synuclein to be a major culprit for PD pathogenesis (Fuchs et al., 2007; Kruger et al., 1998; Polymeropoulos et al., 1997; Spillantini et al., 1997), α-synuclein-derived peptide antigens were found to elicit helper and cytotoxic T cell responses *in vitro* in about 40% of investigated patients with sporadic PD (Sulzer et al., 2017). Human Th17 cells were further shown to induce apoptosis in autologous pluripotent stem cell-derived midbrain neurons (Sommer et al., 2018). Still, ethical considerations preclude any attempt to prove a causal link between α-synuclein peptide-specific T cells and dopaminergic neurodegeneration in humans. Using a mouse model in which PD-like pathology is induced by (over)expression of mutated human α-synuclein in dopaminergic SN neurons, we here describe that dopaminergic neurodegeneration is mediated by antigen-specific T cells. We further identified novel haSyn-derived antigenic peptides recognized by murine T cells.

So far only two studies have compared $CD4^+$ and $CD8^+$ T cell subpopulation in PD brain autopsies with controls, both demonstrating elevated $CD8^+$ T cell counts in PD patients (Brochard et al., 2009; Galiano-Landeira et al., 2020). One study also showed a significant increase of $CD4^+$ T cells (Brochard et al., 2009). In the current study, we

confirmed significantly higher $CD8^+$ T cell numbers within the SN (Galiano-Landeira et al., 2020). In addition, we extended this observation to elevated $CD8^+$ T cell activation markers Granzyme B, KLRG1 and CD107a in human PD SN.

The haSyn PD mouse model was already shown to faithfully recapitulate features of human PD pathophysiology, including dopaminergic endpoints and α-synuclein pathology with insoluble Lewy-like structures (Ip et al., 2017). The increase in T cell numbers in PD patients was mirrored by elevated, $CD8^+$ T cell numbers, in addition to $CD4^+$ T cells in the nigrostriatal tract of haSyn PD mice. The number of T cells was 10-20x higher in haSyn PD mice compared to human PD, pointing towards a stronger immunological reaction in haSyn PD mice. Nevertheless, the observed neuroinflammation could still be considered low-grade compared to the acute MPTP model of PD that demonstrates massively elevated $CD4^+$ and $CD8^+$ T cell infiltrations in the SN, up to ~ 20x higher than observed in haSyn PD mice (Brochard et al., 2009). While human PD displays an even lower level of T cell infiltration, its symptoms only develop over decades. The level of T cell infiltration induced in our mouse model may, in contrast, be sufficient to cause disease formation within months, thereby rendering the haSyn mouse model suitable for use in a research context. A neurotoxic role of $CD4^+$ T cells appears plausible as AAV-encoded α-synuclein, but not AAV-GFP had been shown to enhance MHC II expression, $CD4^+$ T cell proliferation, and numbers of microglial cells in another mouse model for PD (Harms et al., 2013; Theodore et al., 2008; Williams et al., 2021), in which $CD4^{-/-}$ and MHC II knock-out mice were protected from dopaminergic neurodegeneration. The presumed causal role of neuroinflammation in PD is further supported by findings from the rAAV2/7-A53T-aSyn rat model (Van der Perren et al., 2011) where immunosuppression by FK506 treatment reduces T cell infiltration and loss of dopaminergic neurons. Still, the functional role of α-synuclein-specific T cells in neurodegeneration had not been systematically explored before. Transcriptomic data from the immune cell compartment of our haSyn PD mouse model revealed a shift towards a pro-inflammatory milieu in haSyn PD mouse brains indicated by an upregulation of pro-inflammatory genes relevant for both adaptive (in particular T cell-associated) and innate immune functions. The pro-inflammatory genes *Aif1*, *Casp1*, *Jun*, *Sphk1*, *Tnf*, *Trem2*, *Il1b* that had already been linked to PD pathogenesis based on PD cell models, animal models and genetic studies in PD patients (Han et al., 2019; Hu et al., 2019; Koprich et al., 2008; Lindenau et al., 2017; Pyszko and Strosznajder, 2014; Ren et al., 2018; Wang et al., 2016) were found to be upregulated in haSyn PD mice. *Gpnmb*, an anti-inflammatory transmembrane protein that has neuroprotective effects in MPTP mice (Budge et al., 2020), was also induced in haSyn PD mice. Due to elevated protein levels in SN of *post mortem* PD tissue, and based on genome-wide association analyses ((IPDGC, 2011); Moloney et al., 2018) which identified *Gpnmb* as a potential PD risk gene, *Gpnmb* is also implicated in human PD. Based on differentially regulated genes, we finally identified an upregulation of targets of the transcription factors SPI1 and IRF8, which are both linked to microglia activation and possibly to PD (Satoh et al., 2014; Su et al., 2018; Zhou et al., 2019). Gene expression and target enrichment analyses thus indicate an inflammation/repair situation in brains of haSyn PD mice with chronic disease. Deregulations in numerous genes associated with PD underline the high validity of the haSyn PD mouse model.

Focusing on T lymphocytes, we found progressive accumulation of activated $CD4^+CD69^+$ and $CD8^+CD69^+$ T cells in the brains of haSyn PD mice. Consistent with the extracranial origin of other neuroinflammatory diseases (Ferreri et al., 2010), T cells from cervical lymph node display an early and strong upregulation of IL-2 after haSyn vector injection, whereas brain-derived T cells are refractory to stimulation by PMA/ionomycin at that time point. This may be due to an epigenetic adaptation to the normally rather immune-privileged intracranial microenvironment. As meningeal lymphatic vessels drain antigens from the brain into deep cervical lymph nodes (Aspelund et al., 2015; Prinz and Priller, 2017), drainage of haSyn proteins from the brain into cervical lymph nodes may occur shortly after transgene production by the haSyn vector. Lymph node-resident dendritic cells would then process haSyn proteins into immunogenic peptides, as identified by ELISpot assays. Upon antigen-dependent priming, IL-2 then promotes the differentiation of naïve T cells into effector T cells (Boyman and Sprent, 2012). A small population of haSyn-specific memory T cells can then infiltrate the brain, where they are reactivated upon encountering their cognate antigen on neurons (Legroux and Arbour, 2015; Zhan et al., 2017). Accordingly, T cell deficient RAG-$1^{-/-}$ but not B cell deficient $JHD^{-/-}$ haSyn PD mice are protected from motor deficits and loss of dopaminergic neurons, while immunological reconstitution reveals the detrimental roles of $CD4^+$ and - to a lesser, but still significant extent – also $CD8^+$ T cells. However, T and B cells are mutually dependent on each other as $CD4^+$ T helper cells are important for proper activation of B cells. Likewise, $CD4^+$ T and B cells can also support priming and maintenance of cytotoxic $CD8^+$ T cells (Castiglioni et al., 2005; Kumamoto et al., 2011; Linterman et al., 2009). While this calls for a cautious interpretation of our bone marrow reconstitution experiments, it may also explain why these experiments did not reveal one single cell type responsible for neurodegeneration. Similar T cell dependent mechanisms have also been described for other neuroinflammatory diseases such as multiple sclerosis (Legroux and Arbour, 2015), and are apparently responsible for inducing PD-like symptoms in the haSyn PD mouse model.

The notion that PD may be immune-mediated only recently gained strong support when two antigenic regions of human α-synuclein were found to elicit specific T cell responses in PD patients (Sulzer et al., 2017). Strikingly, most PD patients showed MHC II-restricted $CD4^+$ T helper cell-mediated IFN-γ (Th1) and IL-4 (Th2) immune responses, indicating a primarily $CD4^+$ T cell-mediated autoimmune response. In one PD patient, however, T cell responses were mediated by IFN-γ-producing $CD8^+$ T cells (Sulzer et al., 2017). Identification of five haSyn-derived epitopes which specifically induce IFN-γ release in memory T cells from haSyn PD mice implies that a similar situation may be induced by overexpressing mutant haSyn in the SN of mice. Interestingly, one of the identified immunogenic haSyn epitopes (hu_a-Syn120-134) demonstrated an overlap of all but one amino acid with a T cell activating α-synuclein-derived peptide (DNEAYEMPSEEGYQD) that was recently identified as a T cell epitope in PD patients with dementia (Gate et al., 2021).

Further neuronal damage is likely be caused by activated $CD11b^+$ myeloid cells, which were abundantly present in the dopaminergic nigrostriatal tract of haSyn PD mice. A loss of striatal dopaminergic innervation in haSyn PD mice that was even observed in the absence of T cells may be due to reactive oxygen species released by accumulating microglial or infiltrating monocytic cells. The haSyn PD mouse model may thus also allow the investigation of AAV-haSyn induced innate immune pathology which may inflict damage to dopaminergic terminals and axons while sparing the less vulnerable dopaminergic perikarya. Despite intrinsically limited axonal regeneration in adult brains, this would likely result in an (at least partly) repairable neuronal damage. Subsequent induction of T cell-mediated neuronal apoptosis (as shown in Fig. 6) would, however, cause the irreversible loss of dopaminergic neurons. Such a mechanism would also be in line with the growing body of evidence that describes PD as a dying-back neuropathy which starts as an axonopathy followed by neuronal cell body degeneration (Cheng et al., 2010; Doppler et al., 2017; Meissner et al., 2003; Orimo et al., 2008). Despite the lack of protection of striatal fibers and terminals by T cell deficiency in our PD mice, the alleviation of motor deficits could be explained by compensatory adaptation of dopamine turnover in surviving neurons as depicted by a less pronounced HVA/DA ratio in mice either lacking the entire T cell population or $CD4^+$ T cells only.

To demonstrate that T cells from haSyn PD mice induce haSyn antigen-specific neuronal damage, we added mononuclear cells from brains of haSyn PD mice to primary mouse neuron cultures. As different neuronal cells are expected to present ectopically expressed haSyn in a

similar way, we increased the number of available cells (and thus the robustness of our results) by using hippocampal rather than dopaminergic neuron cultures. As an additional advantage, this approach could even expand the scope of our findings beyond PD towards dementia with Lewy bodies (DLB), a disease that is affected by hippocampal α-synuclein aggregations. In DLB, Lewy pathology was dominantly present in the CA2 subregion of the entorhinal cortex (Adamowicz et al., 2017). Moreover, $CD4^+$ T cells were observed in the hippocampus of *post mortem* DLB brains close to vessels, while only a few $CD8^+$ T cells and almost no B cells were found (Iba et al., 2020). To document the loss of neuronal structures by haSyn-activated T cells, we used the somatodendritic marker MAP2. This marker labels neuronal microtubule structures and is suited to document early and late signs of neuronal structure degradation (D'Andrea et al., 2001; Sferra et al., 2020). Use of bulk brain leukocytes rather than purified T cells minimized both *ex vivo* handling of brain-derived immune cells and bias due to preselection of cells. Using this method, we could clearly confirm T cell-induced haSyn-specific neurotoxicity in our mouse model. Antigen-specific damage mediated by the adaptive immune system has been described in several neuroinflammatory diseases such as multiple sclerosis and chronic inflammatory demyelinating polyneuropathy (Diederich et al., 2018; Holz et al., 2000; Kaushansky et al., 2010). It has also been demonstrated for β-synuclein-specific T cells in a novel animal model for multiple sclerosis (Lodygin et al., 2019). Our novel findings now support the notion that PD could be another T cell-mediated autoimmune disease or, at least, a neuroinflammatory disease with a relevant contribution from autoreactive T cells at later time points. Activated microglia might, however, still be the culprits for the T cell-independent loss of striatal dopaminergic innervation observed in haSyn PD mice.

In summary, our findings demonstrate a causal role for α-synuclein specific T cells in PD-associated neurodegeneration and motor dysfunction. The proof of detrimental neuroinflammation in PD has important therapeutic implications. Large randomized controlled, multicentric trials engaging in immune modulation in PD have not been conducted to date. However, several potential immunomodulating agents such as β2-Adrenoceptor agonists or anti-IL-17 therapy have been tried in small open label clinical trials with partially encouraging results (Magistrelli and Comi, 2020; Storelli et al., 2019). A population-based case-control study including approximately 48,000 PD patients and 52,000 controls also analyzed the risk of developing PD with the intake of immunosuppressants. Strikingly, patients medicated with inosine monophosphate dehydrogenase (IMDH) inhibitors had a lower risk for PD. As IMDH inhibitors such as azathioprine and mycophenolate preferentially suppress T cell responses by inhibiting guanosine nucleotide synthesis (Blaheta et al., 1998; Racette et al., 2018), this study supports our conclusion that pro-inflammatory T cell responses represent a new therapeutic target for a disease modifying treatment of human PD. The haSyn PD model now provides an important tool to advance the preclinical and translational work towards new and better immunotherapies for patients with PD.

5. Declarations

5.1. Availability of data and materials

The sequencing datasets generated and analyzed during the current study are available at GEO (http://www.ncbi.nlm.nih.gov/geo) under the accession number GSE148784. All other data generated and analyzed are either included in this published article or available from the corresponding author upon reasonable request.

Funding

This project was supported by the Interdisciplinary Center for Clinical Research (IZKF) at the University of Würzburg (A-303 to C.W.I and M.B.L., A-421 to C.W.I. and J.W., N-362 to C.W.I, project Z-6 to T.H.), by the Nündel-Stiftung (to J.V.), by the Deutsche Stiftung Neurologie and the ParkinsonFonds Germany (to C.W.I.) and by the University Research Funds of the State of Bavaria. Moreover, C.W.I. is supported by the Deutsche Forschungsgemeinschaft (DFG, German Research Foundation) Project-ID 424778381-TRR 295 (A06) and the VERUM Foundation. J.V. has received funding from the European Union's Horizon 2020 research and innovation programme under the EJP RD COFUND-EJP N° 825,575 (EurDyscover), the Nündel Stiftung and the DFG Project-ID 424778381-TRR 295 (A01). R.B. was funded by the DFG BL567/3–2 and the DFG Project-ID 424778381-TRR 295 (A02). A.A.K. was funded by the MoE Ghana/DAAD. R.L.M was funded by the Alexander von Humboldt-Stiftung. This publication was supported by the Open Access Publication Fund of the University of Würzburg.

Author contributions

C.W.I. developed the concept of this study and designed the study; C.W.I., M.B.L., J.W. and A.A.K. wrote the manuscript; C.W.I., A.A.K., E.R., M.G., S.K., B.H., J.B.K., R.B., V.B., F.A., C.M.M., U.K., R.L.M., R.Y., T.H. performed experiments and analyzed data; C.W.I., J.W., J.M.B., A.P., M.B.L., J.V. interpreted the data. The authors have declared that no conflict of interest exists.

Acknowledgments

We thank the Core Unit SysMed at the University of Würzburg for excellent technical support and RNA-seq data generation. The authors are grateful to Louisa Frieß, Heike Menzel, Veronika Senger and Marion Heuer for expert technical assistance.

Appendix A. Supplementary data

Supplementary data to this article can be found online at https://doi.org/10.1016/j.bbi.2022.01.007.

References

(IPDGC), I.P.s.D.G.C., 2011. A two-stage meta-analysis identifies several new loci for Parkinson's disease. PLoS Genet 7, e1002142.

Abeliovich, A., Schmitz, Y., Farinas, I., Choi-Lundberg, D., Ho, W.H., Castillo, P.E., Shinsky, N., Verdugo, J.M., Armanini, M., Ryan, A., Hynes, M., Phillips, H., Sulzer, D., Rosenthal, A., 2000. Mice lacking alpha-synuclein display functional deficits in the nigrostriatal dopamine system. Neuron 25, 239–252.

Adamowicz, D.H., Roy, S., Salmon, D.P., Galasko, D.R., Hansen, L.A., Masliah, E., Gage, F.H., 2017. Hippocampal α-Synuclein in Dementia with Lewy Bodies Contributes to Memory Impairment and Is Consistent with Spread of Pathology. J Neurosci 37 (7), 1675–1684.

Aspelund, A., Antila, S., Proulx, S.T., Karlsen, T.V., Karaman, S., Detmar, M., Wiig, H., Alitalo, K., 2015. A dural lymphatic vascular system that drains brain interstitial fluid and macromolecules. J Exp Med 212, 991–999.

Baba, Y., Kuroiwa, A., Uitti, R.J., Wszolek, Z.K., Yamada, T., 2005. Alterations of T-lymphocyte populations in Parkinson disease. Parkinsonism Relat Disord 11 (8), 493–498.

Bas, J., Calopa, M., Mestre, M., Mollevi, D.G., Cutillas, B., Ambrosio, S., Buendia, E., 2001. Lymphocyte populations in Parkinson's disease and in rat models of parkinsonism. J Neuroimmunol 113, 146–152.

Bendor, J.T., Logan, T.P., Edwards, R.H., 2013. The function of alpha-synuclein. Neuron 79, 1044–1066.

Blaheta, R.A., Leckel, K., Wittig, B., Zenker, D., Oppermann, E., Harder, S., Scholz, M., Weber, S., Schuldes, H., Encke, A., Markus, B.H., 1998. Inhibition of endothelial receptor expression and of T-cell ligand activity by mycophenolate mofetil. Transpl Immunol 6 (4), 251–259.

Boyman, O., Sprent, J., 2012. The role of interleukin-2 during homeostasis and activation of the immune system. Nat Rev Immunol 12 (3), 180–190.

Braak, H., Ghebremedhin, E., Rüb, U., Bratzke, H., Del Tredici, K., 2004. Stages in the development of Parkinson's disease-related pathology. Cell Tissue Res 318 (1), 121–134.

Brochard, V., Combadiere, B., Prigent, A., Laouar, Y., Perrin, A., Beray-Berthat, V., Bonduelle, O., Alvarez-Fischer, D., Callebert, J., Launay, J.M., Duyckaerts, C., Flavell, R.A., Hirsch, E.C., Hunot, S., 2009. Infiltration of CD4+ lymphocytes into the brain contributes to neurodegeneration in a mouse model of Parkinson disease. J Clin Invest 119, 182–192.

Budge, K., Neal, M., Richardson, J., Safadi, F., 2020. Transgenic Overexpression of GPNMB Protects Against MPTP-Induced Neurodegeneration. Mol Neurobiol 33 (S1). https://doi.org/10.1096/fsb2.v33.S110.1096/fasebj.2019.33.1_supplement.662.7.

Castiglioni, P., Gerloni, M., Cortez-Gonzalez, X., Zanetti, M., 2005. CD8 T cell priming by B lymphocytes is CD4 help dependent. Eur J Immunol 35 (5), 1360–1370.
Chen, E.Y., Tan, C.M., Kou, Y., Duan, Q., Wang, Z., Meirelles, G.V., Clark, N.R., Ma'ayan, A., 2013. Enrichr: interactive and collaborative HTML5 gene list enrichment analysis tool. BMC Bioinformatics 14, 128.
Chen, Z., Huang, A., Sun, J., Jiang, T., Qin, F.X., Wu, A., 2017. Inference of immune cell composition on the expression profiles of mouse tissue. Sci Rep 7, 40508.
Chen, Z., Quan, L., Huang, A., Zhao, Q., Yuan, Y., Yuan, X., Shen, Q., Shang, J., Ben, Y., Qin, F.-F., Wu, A., 2018. seq-ImmuCC: Cell-Centric View of Tissue Transcriptome Measuring Cellular Compositions of Immune Microenvironment From Mouse RNA-Seq Data. Front Immunol 9. https://doi.org/10.3389/fimmu.2018.0128610.3389/fimmu.2018.01286.s00110.3389/fimmu.2018.01286.s00210.3389/fimmu.2018.01286.s003.
Cheng, H.-C., Ulane, C.M., Burke, R.E., 2010. Clinical progression in Parkinson disease and the neurobiology of axons. Ann Neurol 67 (6), 715–725.
D'Andrea, M.R., Ilyin, S., Plata-Salaman, C.R., 2001. Abnormal patterns of microtubule-associated protein-2 (MAP-2) immunolabeling in neuronal nuclei and Lewy bodies in Parkinson's disease substantia nigra brain tissues. Neurosci Lett 306 (3), 137–140.
Dauer, W., Przedborski, S., 2003. Parkinson's disease: mechanisms and models. Neuron 39 (6), 889–909.
Diederich, J.M., Staudt, M., Meisel, C., Hahn, K., Meinl, E., Meisel, A., Klehmet, J., 2018. Neurofascin and Compact Myelin Antigen-Specific T Cell Response Pattern in Chronic Inflammatory Demyelinating Polyneuropathy Subtypes. Front Neurol 9, 171.
Dobin, A., Davis, C.A., Schlesinger, F., Drenkow, J., Zaleski, C., Jha, S., Batut, P., Chaisson, M., Gingeras, T.R., 2013. STAR: ultrafast universal RNA-seq aligner. Bioinformatics 29, 15-21.
Doppler, K., Jentschke, H.M., Schulmeyer, L., Vadasz, D., Janzen, A., Luster, M., Hoffken, H., Mayer, G., Brumberg, J., Booij, J., Musacchio, T., Klebe, S., Sittig-Wiegand, E., Volkmann, J., Sommer, C., Oertel, W.H., 2017. Dermal phospho-alpha-synuclein deposits confirm REM sleep behaviour disorder as prodromal Parkinson's disease. Acta Neuropathol 133, 535-545.
Ferreri, A.J.M., Illerhaus, G., Zucca, E., Cavalli, F., 2010. Flows and flaws in primary central nervous system lymphoma. Nat Rev Clin Oncol 7 (8), 1–2.
Fuchs, J., Nilsson, C., Kachergus, J., Munz, M., Larsson, E.-M., Schüle, B., Langston, J.W., Middleton, F.A., Ross, O.A., Hulihan, M., Gasser, T., Farrer, M.J., 2007. Phenotypic variation in a large Swedish pedigree due to SNCA duplication and triplication. Neurology 68 (12), 916–922.
Fujiwara, H., Hasegawa, M., Dohmae, N., Kawashima, A., Masliah, E., 2002. alpha-synuclein is phosphorylated in synucleinopathy lesions. Nat. Cell Biol. 4, 160.
Galiano-Landeira, J., Torra, A., Vila, M., Bové, J., 2020. CD8 T cell nigral infiltration precedes synucleinopathy in early stages of Parkinson's disease. Brain 143, 3717-3733.
Gate, D., Tapp, E., Leventhal, O., Shahid, M., Nonninger, T.J., Yang, A.C., Strempfl, K., Unger, M.S., Fehlmann, T., Oh, H., Channappa, D., Henderson, V.W., Keller, A., Aigner, L., Galasko, D.R., Davis, M.M., Poston, K.L., Wyss-Coray, T., 2021. CD4(+) T cells contribute to neurodegeneration in Lewy body dementia. Science 374 (6569), 868–874.
Han, X., Sun, S., Sun, Y., Song, Q., Zhu, J., Song, N., Chen, M., Sun, T., Xia, M., Ding, J., Lu, M., Yao, H., Hu, G., 2019. Small molecule-driven NLRP3 inflammation inhibition via interplay between ubiquitination and autophagy: implications for Parkinson disease. Autophagy 15 (11), 1860–1881.
Harms, A.S., Cao, S., Rowse, A.L., Thome, A.D., Li, X., Mangieri, L.R., Cron, R.Q., Shacka, J.J., Raman, C., Standaert, D.G., 2013. MHCII is required for α-synuclein-induced activation of microglia, CD4 T cell proliferation, and dopaminergic neurodegeneration. J Neurosci 33, 9592–9600.
Hernandez, D.G., Reed, X., Singleton, A.B., 2016. Genetics in Parkinson disease: Mendelian versus non-Mendelian inheritance. J Neurochem 139 (Suppl 1), 59–74.
Holz, A., Bielekova, B., Martin, R., Oldstone, M.B.A., 2000. Myelin-associated oligodendrocytic basic protein: identification of an encephalitogenic epitope and association with multiple sclerosis. J Immunol 164 (2), 1103–1109.
Hu, K., Huang, Q., Liu, C., Li, Y., Liu, Y., Wang, H., Li, M., Ma, S., 2019. c-Jun/Bim Upregulation in Dopaminergic Neurons Promotes Neurodegeneration in the MPTP Mouse Model of Parkinson's Disease. Neuroscience 399, 117–124.
Iba, M., Kim, C., Sallin, M., Kwon, S., Verma, A., Overk, C., Rissman, R.A., Sen, R., Sen, J. M., Masliah, E., 2020. Neuroinflammation is associated with infiltration of T cells in Lewy body disease and α-synuclein transgenic models. J Neuroinflammation 17, 214.
Ip, C.W., Beck, S.K., Volkmann, J., 2015. Lymphocytes reduce nigrostriatal deficits in the 6-hydroxydopamine mouse model of Parkinson's disease. J Neural Transm (Vienna) 122 (12), 1633–1643.
Ip, C.W., Klaus, L.C., Karikari, A.A., Visanji, N.P., Brotchie, J.M., Lang, A.E., Volkmann, J., Koprich, J.B., 2017. AAV1/2-induced overexpression of A53T-alpha-synuclein in the substantia nigra results in degeneration of the nigrostriatal system with Lewy-like pathology and motor impairment: a new mouse model for Parkinson's disease. Acta Neuropathol Commun 5, 11.
Kaushansky, N., Eisenstein, M., Zilkha-Falb, R., Ben-Nun, A., 2010. The myelin-associated oligodendrocytic basic protein (MOBP) as a relevant primary target autoantigen in multiple sclerosis. Autoimmun Rev 9 (4), 233–236.
Koprich, J.B., Reske-Nielsen, C., Mithal, P., Isacson, O., 2008. Neuroinflammation mediated by IL-1beta increases susceptibility of dopamine neurons to degeneration in an animal model of Parkinson's disease. J Neuroinflammation 5, 8.
Kruger, R., Kuhn, W., Muller, T., Woitalla, D., Graeber, M., Kosel, S., Przuntek, H., Epplen, J.T., Schols, L., Riess, O., 1998. Ala30Pro mutation in the gene encoding alpha-synuclein in Parkinson's disease. Nat Genet 18, 106–108.
Kuleshov, M.V., Jones, M.R., Rouillard, A.D., Fernandez, N.F., Duan, Q., Wang, Z., Koplev, S., Jenkins, S.L., Jagodnik, K.M., Lachmann, A., McDermott, M.G., Monteiro, C.D., Gundersen, G.W., Ma'ayan, A., 2016. Enrichr: a comprehensive gene set enrichment analysis web server 2016 update. Nucleic Acids Res 44 (W1), W90–W97.
Kumamoto, Y., Mattei, L.M., Sellers, S., Payne, G.W., Iwasaki, A., 2011. CD4+ T cells support cytotoxic T lymphocyte priming by controlling lymph node input. Proceedings of the National Academy of Sciences 108 (21), 8749–8754.
Lang, A.E., Lozano, A.M., 1998. Parkinson's disease. First of two parts. N Engl J Med 339 (15), 1044–1053.
Legroux, L., Arbour, N., 2015. Multiple Sclerosis and T Lymphocytes: An Entangled Story. J Neuroimmune Pharmacol 10 (4), 528–546.
Liao, Y., Smyth, G.K., Shi, W., 2014. featureCounts: an efficient general purpose program for assigning sequence reads to genomic features. Bioinformatics 30 (7), 923–930.
Lindenau, J.D., Altmann, V., Schumacher-Schuh, A.F., Rieder, C.R., Hutz, M.H., 2017. Tumor necrosis factor alpha polymorphisms are associated with Parkinson's disease age at onset. Neurosci Lett 658, 133–136.
Lindestam Arlehamn, C.S., Dhanwani, R., Pham, J., Kuan, R., Frazier, A., Rezende Dutra, J., Phillips, E., Mallal, S., Roederer, M., Marder, K.S., Amara, A.W., Standaert, D.G., Goldman, J.G., Litvan, I., Peters, B., Sulzer, D., Sette, A., 2020. α-Synuclein-specific T cell reactivity is associated with preclinical and early Parkinson's disease. Nat Commun 11, 1875.
Linterman, M.A., Rigby, R.J., Wong, R.K., Yu, D., Brink, R., Cannons, J.L., Schwartzberg, P.L., Cook, M.C., Walters, G.D., Vinuesa, C.G., 2009. Follicular helper T cells are required for systemic autoimmunity. Journal of Experimental Medicine 206, 561–576.
Lodygin, D., Hermann, M., Schweingruber, N., Flügel-Koch, C., Watanabe, T., Schlosser, C., Merlini, A., Körner, H., Chang, H.-F., Fischer, H.J., Reichardt, H.M., Zagrebelsky, M., Mollenhauer, B., Kügler, S., Fitzner, D., Frahm, J., Stadelmann, C., Haberl, M., Odoardi, F., Flügel, A., 2019. β-Synuclein-reactive T cells induce autoimmune CNS grey matter degeneration. Nature 566 (7745), 503–508.
Love, M.I., Huber, W., Anders, S., 2014. Moderated estimation of fold change and dispersion for RNA-seq data with DESeq2. Genome Biol 15, 550.
Magistrelli, L., Comi, C., 2020. Beta2-Adrenoceptor Agonists in Parkinson's Disease and Other Synucleinopathies. J Neuroimmune Pharmacol 15 (1), 74–81.
Marsden, C.D., 1990. Parkinson's disease. Lancet 335 (8695), 948–949.
McGeer, P.L., Itagaki, S., Boyes, B.E., McGeer, E.G., 1988. Reactive microglia are positive for HLA-DR in the substantia nigra of Parkinson's and Alzheimer's disease brains. Neurology 38, 1285-1291.
Meissner, W., Prunier, C., Guilloteau, D., Chalon, S., Gross, C.E., Bezard, E., 2003. Time-course of nigrostriatal degeneration in a progressive MPTP-lesioned macaque model of Parkinson's disease. Mol Neurobiol 28 (3), 209–218.
Mogi, M., Harada, M., Kondo, T., Riederer, P., Inagaki, H., Minami, M., Nagatsu, T., 1994a. Interleukin-1 beta, interleukin-6, epidermal growth factor and transforming growth factor-alpha are elevated in the brain from parkinsonian patients. Neurosci Lett 180, 147–150.
Mogi, M., Harada, M., Riederer, P., Narabayashi, H., Fujita, K., Nagatsu, T., 1994b. Tumor necrosis factor-alpha (TNF-alpha) increases both in the brain and in the cerebrospinal fluid from parkinsonian patients. Neurosci Lett 165, 208–210.
Moloney, E.B., Moskites, A., Ferrari, E.J., Isacson, O., Hallett, P.J., 2018. The glycoprotein GPNMB is selectively elevated in the substantia nigra of Parkinson's disease patients and increases after lysosomal stress. Neurobiol Dis 120, 1–11.
Orimo, S., Uchihara, T., Nakamura, A., Mori, F., Kakita, A., Wakabayashi, K., Takahashi, H., 2008. Axonal α-synuclein aggregates herald centripetal degeneration of cardiac sympathetic nerve in Parkinson's disease. Brain 131, 642–650.
Page, N., Lemeille, S., Vincenti, I., Klimek, B., Mariotte, A., Wagner, I., Di Liberto, G., Kaye, J., Merkler, D., 2021. Persistence of self-reactive CD8+ T cells in the CNS requires TOX-dependent chromatin remodeling. Nat Commun 12, 1009.
Polymeropoulos, M.H., Lavedan, C., Leroy, E., Ide, S.E., Dehejia, A., Dutra, A., Pike, B., Root, H., Rubenstein, J., Boyer, R., Stenroos, E.S., Chandrasekharappa, S., Athanassiadou, A., Papapetropoulos, T., Johnson, W.G., Lazzarini, A.M., Duvoisin, R. C., Di Iorio, G., Golbe, L.I., Nussbaum, R.L., 1997. Mutation in the alpha-Synuclein Gene Identified in Families with Parkinson's Disease. Science 276, 2045–2047.
Prinz, M., Priller, J., 2017. The role of peripheral immune cells in the CNS in steady state and disease. Nat Neurosci 20 (2), 136–144.
Pyszko, J.A., Strosznajder, J.B., 2014. The key role of sphingosine kinases in the molecular mechanism of neuronal cell survival and death in an experimental model of Parkinson's disease. Folia Neuropathol 52, 260–269.
Racette, B.A., Gross, A., Vouri, S.M., Camacho-Soto, A., Willis, A.W., Searles Nielsen, S., 2018. Immunosuppressants and risk of Parkinson disease. Ann Clin Transl Neurol 5 (7), 870–875.
Ren, M., Guo, Y., Wei, X., Yan, S., Qin, Y., Zhang, X., Jiang, F., Lou, H., 2018. TREM2 overexpression attenuates neuroinflammation and protects dopaminergic neurons in experimental models of Parkinson's disease. Exp Neurol 302, 205–213.
Reynolds, A.D., Stone, D.K., Hutter, J.A.L., Benner, E.J., Mosley, R.L., Gendelman, H.E., 2010. Regulatory T cells attenuate Th17 cell-mediated nigrostriatal dopaminergic neurodegeneration in a model of Parkinson's disease. J Immunol 184 (5), 2261–2271.
Ross, G.W., Petrovitch, H., Abbott, R.D., Nelson, J., Markesbery, W., Davis, D., Hardman, J., Launer, L., Masaki, K., Tanner, C.M., White, L.R., 2004. Parkinsonian signs and substantia nigra neuron density in decendents elders without PD. Ann Neurol 56 (4), 532–539.
Satoh, J., Asahina, N., Kitano, S., Kino, Y., 2014. A Comprehensive Profile of ChIP-Seq-Based PU.1/Spi1 Target Genes in Microglia. Gene Regul Syst Bio 8, 127–139.
Saunders, J.A.H., Estes, K.A., Kosloski, L.M., Allen, H.E., Dempsey, K.M., Torres-Russotto, D.R., Meza, J.L., Santamaria, P.M., Bertoni, J.M., Murman, D.L., Ali, H.H.,

Standaert, D.G., Mosley, R.L., Gendelman, H.E., 2012. CD4+ regulatory and effector/memory T cell subsets profile motor dysfunction in Parkinson's disease. J Neuroimmune Pharmacol 7 (4), 927–938.

Sferra, A., Nicita, F., Bertini, E., 2020. Microtubule Dysfunction: A Common Feature of Neurodegenerative Diseases. International journal of molecular sciences 21.

Sommer, A., Marxreiter, F., Krach, F., Fadler, T., Grosch, J., Maroni, M., Graef, D., Eberhardt, E., Riemenschneider, M.J., Yeo, G.W., Kohl, Z., Xiang, W., Gage, F.H., Winkler, J., Prots, I., Winner, B., 2018. Th17 Lymphocytes Induce Neuronal Cell Death in a Human iPSC-Based Model of Parkinson's Disease. Cell Stem Cell 23 (1), 123–131.e6.

Spillantini, M.G., Schmidt, M.L., Lee, V.M., Trojanowski, J.Q., Jakes, R., Goedert, M., 1997. Alpha-synuclein in Lewy bodies. Nature 388, 839–840.

Storelli, E., Cassina, N., Rasini, E., Marino, F., Cosentino, M., 2019. Do Th17 Lymphocytes and IL-17 Contribute to Parkinson's Disease? A Systematic Review of Available Evidence. Front Neurol 10, 13.

Su, L., Wang, C., Zheng, C., Wei, H., Song, X., 2018. A meta-analysis of public microarray data identifies biological regulatory networks in Parkinson's disease. BMC Med Genomics 11, 40.

Sulzer, D., Alcalay, R.N., Garretti, F., Cote, L., Kanter, E., Agin-Liebes, J., Liong, C., McMurtrey, C., Hildebrand, W.H., Mao, X., Dawson, V.L., Dawson, T.M., Oseroff, C., Pham, J., Sidney, J., Dillon, M.B., Carpenter, C., Weiskopf, D., Phillips, E., Mallal, S., Peters, B., Frazier, A., Lindestam Arlehamn, C.S., Sette, A., 2017. T cells from patients with Parkinson's disease recognize alpha-synuclein peptides. Nature 546, 656–661.

Theodore, S., Cao, S., McLean, P.J., Standaert, D.G., 2008. Targeted overexpression of human alpha-synuclein triggers microglial activation and an adaptive immune response in a mouse model of Parkinson disease. J Neuropathol Exp Neurol 67, 1149–1158.

Van der Perren, A., Toelen, J., Carlon, M., Van den Haute, C., Coun, F., Heeman, B., Reumers, V., Vandenberghe, L.H., Wilson, J.M., Debyser, Z., Baekelandt, V., 2011. Efficient and stable transduction of dopaminergic neurons in rat substantia nigra by rAAV 2/1, 2/2, 2/5, 2/6.2, 2/7, 2/8 and 2/9. Gene Ther 18 (5), 517–527.

Wang, W., Nguyen, L.T.T., Burlak, C., Chegini, F., Guo, F., Chataway, T., Ju, S., Fisher, O. S., Miller, D.W., Datta, D., Wu, F., Wu, C.-X., Landeru, A., Wells, J.A., Cookson, M.R., Boxer, M.B., Thomas, C.J., Gai, W.P., Ringe, D., Petsko, G.A., Hoang, Q.Q., 2016. Caspase-1 causes truncation and aggregation of the Parkinson's disease-associated protein α-synuclein. Proc Natl Acad Sci U S A 113 (34), 9587–9592.

Williams, G.P., Schonhoff, A.M., Jurkuvenaite, A., Gallups, N.J., Standaert, D.G., Harms, A.S., 2021. CD4 T cells mediate brain inflammation and neurodegeneration in a mouse model of Parkinson disease. Brain 144, 2047–2059.

Yu, G., Wang, L.-G., Han, Y., He, Q.-Y., 2012. clusterProfiler: an R package for comparing biological themes among gene clusters. OMICS 16 (5), 284–287.

Zhan, Y., Carrington, E.M., Zhang, Y., Heinzel, S., Lew, A.M., 2017. Life and Death of Activated T Cells: How Are They Different from Naive T Cells? Front Immunol 8, 1809.

Zhou, N., Liu, K., Sun, Y., Cao, Y., Yang, J., 2019. Transcriptional mechanism of IRF8 and PU.1 governs microglial activation in neurodegenerative condition. Protein Cell 10 (2), 87–103.